Quantitative Protein and mRNA Profiling Shows Selective Post-Transcriptional Control of Protein Expression by Vasopressin in Kidney Cells*[S]

Sookkasem Khositseth‡, Trairak Pisitkun‡, Dane H. Slentz‡, Guanghui Wang‡, Jason D. Hoffert‡, Mark A. Knepper‡, and Ming-Jiun Yu‡§

Previous studies in yeast have supported the view that post-transcriptional regulation of protein abundances may be more important than previously believed. Here we ask the question: "*In a physiological regulatory process (the response of mammalian kidney cells to the hormone vasopressin), what fraction of the expressed proteome undergoes a change in abundance and what fraction of the regulated proteins have corresponding changes in mRNA levels?*" In humans and other mammals, vasopressin fulfills a vital homeostatic role (*viz.* regulation of renal water excretion) by regulating the water channel aquaporin-2 in collecting duct cells. To address the question posed, we utilized large-scale quantitative protein mass spectrometry (LC-MS/MS) employing stable isotopic labeling in cultured mpkCCD cells ('SILAC') coupled with transcriptomic profiling using oligonucleotide expression arrays (Affymetrix). Preliminary studies analyzing two nominally identical control samples by SILAC LC-MS/MS yielded a relative S.D. of 13% (for ratios), establishing the precision of the SILAC approach in our hands. We quantified nearly 3000 proteins with nontargeted SILAC LC-MS/MS, comparing vasopressin- *versus* vehicle-treated samples. Of these proteins 786 of them were quantified in each of 3 experiments, allowing statistical analysis and 188 of these showed significant vasopressin-induced changes in abundance, including aquaporin-2 (20-fold increase). Among the proteins with statistically significant abundance changes, a large fraction (at least one-third) was found to lack changes in the corresponding mRNA species (despite sufficient statistical power), indicating that post-transcriptional regulation of protein abundance plays an important role in the vasopressin response. Bioinformatic analysis of the regulated proteins (*versus* all transcripts) shows enrichment of glutathione S-transferase isoforms as well as proteins involved in organization of the actin cytoskeleton. The latter suggests that long-term regulatory processes may contribute to actomyosin-dependent trafficking of the water channel aquaporin-2. The results provide impetus for increased focus on translational regulation and regulation of protein degradation in physiological control in mammalian epithelial cells. ***Molecular & Cellular Proteomics 10: 10.1074/mcp.M110.004036, 1–21, 2011.***

In multicellular organisms, the phenotypes of individual cell types are specified by the subset of protein-coding genes that are expressed. Control of function is in part determined by selective regulation of the abundances of the expressed proteins. Protein abundances are determined by transcriptional as well as post-transcriptional processes. The latter consists of control of translation rate and control of protein degradation. Previous studies examining responses to metabolic perturbations in yeast, a unicellular eukaryotic organism, have supported the view that post-transcriptional regulation of protein abundances may be more important than previously believed (1–3). Here we ask the question: "*In a physiological regulatory process in a differentiated mammalian cell type (response to the hormone vasopressin in mammalian kidney cells), what fraction of the expressed proteome undergoes a change in abundance and what fraction of the regulated proteins have changes in corresponding mRNA levels?*"

In mammals, the peptide hormone vasopressin regulates water excretion, thereby maintaining tight control of whole-animal water balance. Control of renal water excretion is achieved predominantly by the action of vasopressin to regulate the molecular water channel, *aquaporin-2* (Gene symbol: *Aqp2*) in renal collecting duct cells (4). Vasopressin regulates aquaporin-2 in two ways: a) by evoking membrane-trafficking events that move aquaporin-2 from the intracellular compartment to the apical plasma membrane of collecting duct cells; and b) by increasing the overall abundance of the aquaporin-2 protein in collecting duct cells. The former event occurs in seconds to minutes (5), whereas the later event takes hours to days (6). These two processes combine to increase the abundance of aquaporin-2 in the plasma membrane, rendering the cell perme-

From the ‡Epithelial Systems Biology Laboratory, NHLBI, National Institutes of Health, Bethesda, MD 20892-1603, USA

Received August 6, 2010, and in revised form, October 8, 2010
Published, MCP Papers in Press, October 12, 2010, DOI 10.1074/mcp.M110.004036

able to water and increasing osmotic water transport from the forming urine back into the blood.

Vasopressin exerts its actions in collecting duct cells by binding to V2 subtype vasopressin receptors (*Avpr2*), which are coupled to adenylyl cyclases III and VI (*Adcy3* and *Adcy6*) (7) via the heterotrimeric G-protein $G_s\alpha$ (*Gnas*), thereby increasing cyclic AMP levels. Vasopressin also stimulates calcium mobilization in the form of aperiodic calcium spikes (8, 9) that control aquaporin-2 trafficking through calmodulin-mediated regulation of myosin light chain kinase (*Mylk*) (10, 11). This kinase regulates the activity of nonmuscle myosin II isoforms (*Myh9* and *Myh10*) in the collecting duct cells in association with changes in the distribution of filamentous actin (F-actin). Regulation of the actin cytoskeleton in collecting duct cells by vasopressin has been inferred from studies showing attenuation of F-actin near the apical plasma membrane (12) and an increase in the deformability of the apical plasma membrane (13), presumably because of modification of the properties of the cytoskeleton. These changes appear to be mediated in part by the ability of vasopressin to activate isoforms of the small GTP-binding protein *rho (Rhoa* and *Rhob*) (14, 15). In addition, tropomyosin-1, bound to the aquaporin-2-containing endosomes, causes local F-actin depolymerization, which may reduce the cortical actin barrier to vesicle translocation (16). Our understanding of the overall mechanism of aquaporin-2 regulation is, however, incomplete.

The process of discovery in biology has been abetted by the recent availability of comprehensive genome sequence data for a variety of organisms, generated as a product of genome sequencing projects. The availability of such data has made possible a variety of large-scale methodologies such as protein mass spectrometry and oligonucleotide arrays, which permit large-scale profiling of proteins and the transcripts that code for them in specific cell types. Here we apply both of these methods to the understanding of the long-term effects of vasopressin on aquaporin-2-expressing cultured mouse collecting duct cells (mpkCCD clone 11 (17)). We use stable isotopic labeling in cultured mpkCCD cells (the so-called "SILAC"[1] method (18)) coupled to liquid chromatography-tandem MS (LC-MS/MS) for large-scale quantification of changes in protein abundance, paired with Affymetrix oligonucleotide microarrays to assess changes in the corresponding mRNA transcript levels. The LC-MS/MS results confirm that vasopressin exposure of collecting duct cells triggers a large increase in aquaporin-2 protein abundance. They also identify 101 other proteins that undergo significant increases in protein abundance in response to vasopressin as well as 86 that significantly decrease. Surprisingly a large fraction of the regulated proteins lacked changes in abundances of the corresponding mRNA transcripts despite adequate statistical power, suggesting that, in this physiological system, post-transcriptional regulation of protein abundance is more prevalent than previously believed.

EXPERIMENTAL PROCEDURES

Cell Culture—Clone 11 mpkCCD cells (17) were maintained in Dulbecco's modified Eagle's medium:Ham's F_{12} medium plus supplements and 2% fetal bovine serum at 37 °C with 5% CO_2 and 95% air. In general, ~20,000 cells per cm^2 were plated on membrane supports with daily monitoring of transepithelial resistance. Once transepithelial resistance reached 5 $k\Omega \cdot cm^2$ indicating confluence, the cells were exposed to the vasopressin V2 receptor-selective agonist 1-desamino-8-D-arginine-vasopressin (dDAVP) (0.1 nM) or vehicle added to the basolateral medium (deprived of serum, hormones, and growth factors except transferrin and selenate). The apical aspect of cells was exposed to the same medium, but lacking dDAVP. Apical and basolateral media were changed daily.

Immunoblotting—After washing twice with phosphate-buffered saline, proteins were harvested in SDS-sample buffer (2% SDS, 50 mM Tris, pH 6.8) plus protease inhibitors. Protein concentrations were measured using the bicinchoninic acid protein assay (23225, Thermo Fisher Scientific Inc., Waltham, MA). The remaining immunoblotting procedures were as described previously (19) and images were developed and quantified using near-infrared fluorescence (Li-Cor Odyssey, Lincoln, Nebraska). Equal protein loading was confirmed on parallel Coomassie blue-stained SDS-PAGE gels.

The rabbit polyclonal antibody to aquaporin-2 was previously generated in our laboratory (20). The antibody to Mal2 was previously characterized (21). Commercial antibodies were to Actn4 (SC-134236) (Santa Cruz Biotechnology, Santa Cruz, CA); Akap12 (G3795) (Sigma-Aldrich); Add1 (SC-25731) (Santa Cruz); Car2 (16961–1-AP) (Proteintech, Chicago, IL); Capg (10194–1-AP) (Proteintech); Ctsd (SC-6486) (Santa Cruz); Flii (SC-21716) (Santa Cruz); Gsn (ab74420) (Abcam, Boston, MA); Itgb1 (4706) (Cell Signaling, Beverly, MA); Lima (NB100–2305) (Novus, Littleton, CO); Macf1 (H00023499-A01) (Abnova, Taipei, Taiwan); Nherf1 (PA1090) (Affinity Bioreagents, Golden, CO); Spnb2 (612562) (BD Bioscience); Tgm2 (06–471) (Millipore). Species-specific secondary antibodies were obtained from Molecular Probes (Invitrogen).

Stable Isotopic Labeling by Amino Acids in Cell Culture (SILAC)—The mpkCCD cells were cultured in "heavy" or "light" medium containing advanced Dulbecco's modified Eagle's medium/F_{12} base medium (12634–010) (Invitrogen Corp. Carlsbad, CA) with 2% dialyzed serum (MS10033) (Invitrogen) plus heavy or light lysine and arginine (MS10009) (Invitrogen). "Light" amino acids were [$^{12}C_6$]-lysine (91 mg/L) and [$^{12}C_6$, $^{14}N_4$]-arginine (147 mg/L). "Heavy" amino acids were [$^{13}C_6$]-lysine (91 mg/L)) and 147 mg/L [$^{13}C_6$, $^{15}N_4$]-arginine (147 mg/L). The superscripts denote atomic mass of carbon (C) and nitrogen (N), whereas the subscripts denote numbers of labeled atoms in the amino acids. Heavy medium or light medium was used for the "vasopressin-treated" cells in alternating fashion in different experiments. Peptides labeled with heavy amino acids obtain an extra mass of 6.02 or 10.01 Da, respectively, for each heavy lysine or arginine, which allows the sample of origin to be distinguished by the mass spectrometer and relative abundances to be assigned to vasopressin-treated *versus* vehicle-treated cells based on MS1 peak intensity.

To test amino acid incorporation, 50 μg of protein from cells grown in light and heavy media for 7 or 12 days were extracted, mixed at a 1:1 ratio, and processed for LC-MS/MS peptide identification and

[1] The abbreviations used are: SILAC, stable isotopic labeling by amino acids in cell culture; dDAVP, 1-desamino-8-d-arginine-vasopressin; FA, formic acid; Nherf1, sodium/hydrogen exchanger regulatory factor 1; LC-MS/MS, liquid chromatography-tandem MS; ACN, acetonitrile; MRM, multiple-reaction monitoring; ARE, antioxidant regulatory elements.

quantification. Complete incorporation of isotopic amino acids is expected to yield a unity abundance ratio of light to heavy peptides in a 1:1 mixed protein sample. Sixty-one peptides from cells grown in the light and the heavy media for 7 days had an average abundance ratio of 0.99 (Supplemental Table S1), which was not significantly different from unity.

Mammalian cells can theoretically utilize arginine as a precursor for proline (22). If heavy proline was excluded from the search parameters, the abundance of the peptides containing heavy proline would be underestimated, leading to greater light to heavy peptide abundance ratios. To assess the possibility of arginine-to-proline conversion in the mpkCCD cells, we measured the average light to heavy peptide abundance ratios for 22 peptides containing proline and 39 peptides lacking proline from cells cultured with isotopic amino acids for 7 days (Supplemental Table S1). Neither of these two ratios was significantly different from unity, indicating that the mpkCCD cells did not convert arginine to proline in substantial amounts.

One-Dimensional SDS-PAGE and In-Gel Trypsin Digestion—One-dimensional SDS-PAGE and in-gel trypsinization followed previously published methods with minor modifications (23). Briefly, 200 μg of light- and heavy-labeled protein samples were mixed and solubilized with ¼ part of Laemmli buffer (5×: 7.5% SDS, 30% glycerol, 50 mM Tris, pH 6.8) before boiling for 10 min. One-dimensional SDS-PAGE was performed using a 4%–15% gradient polyacrylamide gel. Protein in the gel was visualized with colloidal Coomassie blue staining (GelCode Blue Stain Reagent, G-250; Pierce Biotechnology, Rockford, IL) for 5 min followed by destaining in deionized H_2O for 1 h. Protein in the gel was then sliced into small blocks for a total of 20 or 40 blocks per lane. Each block was minced into small pieces (1–1.5 mm^3). Gel pieces from each block were further destained and dehydrated by incubating with 25 mM NH_4HCO_3/50% acetonitrile (ACN) solution for 10 min three times and then were dried *in vacuo*. Protein in gel pieces was reduced with 10 mM dithiothreitol for 1 h at 56 °C and then alkylated using 55 mM iodoacetamide for 1 h at room temperature in the dark. The gel pieces then were washed with 25 mM NH_4HCO_3 followed by washing with 25 mM NH_4HCO_3/50% ACN twice. The gel pieces then were dried *in vacuo*.

For in-gel trypsin digestion, the dried gel pieces were immersed in 25 mM NH_4HCO_3 solution containing 12.5 ng/μl trypsin (V5113) (Promega Corp., Madison, WI) and incubated at 37 °C overnight. The tryptic peptides were extracted by incubating the gel pieces with 50% ACN/0.1% formic acid (FA) followed by sonication in a water bath for 20 min. This step was repeated twice. The volume of the extracted peptide samples was reduced to about 5 μl *in vacuo* and then the samples were reconstituted to 20 μl of 0.1% FA. The resulting peptide mixtures were concentrated and desalted with C18 Zip-tips (Millipore Corp., Bedford, MA). They were dried *in vacuo* and reconstituted to 10 μl in 0.1% FA for LC-MS/MS analysis.

LC-MS/MS Analysis—Tryptic peptides were analyzed on an Agilent 1100 nanoflow system (Agilent Technologies, Palo Alto, CA) LC connected to an LTQ FT-ICR mass spectrometer (Thermo Fisher Scientific Inc.) equipped with a nano-electrospray ion source. Peptides were loaded onto a peptide trap cartridge (Agilent Technologies) at a flow rate of 4 μl/min. The trapped peptides were then fractionated with reverse-phase PicoFrit column (New Objective, Woburn, MA) using a linear gradient of 0%–60% ACN in 0.1% FA. The gradient time was 120 min at a flow rate of 0.25 μl/min. For protein profiling, both precursor mass (MS1) and fragmented product mass (MS2) were acquired with the LTQ. For peptide quantification, the FT-ICR was used for the MS1 scans and the LTQ was used for the MS2 scans.

Protein Identification and Quantification—Three search algorithms were used to identify peptide ions from the mass spectra, *viz.* Sequest (Bioworks version 3.3.1 SP1) (24), InsPecT (version 20081014) (25), and OMSSA (version 2.1.4) (26). For the Sequest and OMSSA search algorithms, the peak lists (dta files) were generated from the RAW files using Bioworks software. The criteria were: precursor mass range between 600 and 3500 amu, precursor tolerance = 1.4 amu for grouping spectra, a total ion current > 1000 (arbitrary unit) per spectrum, and a minimum of 15 peaks per spectrum. For the InsPecT search algorithm, the RAW files were converted to mzXML files without filtering. The search parameters included precursor ion mass tolerance = 1.5 amu, and fragment product ion mass accuracy = 1.0 amu for LTQ spectra. For FT-ICR spectra, the precursor mass tolerance was 50 ppm and the product mass was 1.0 amu. A single fixed modification was carbamidomethylation of cysteine (+57), whereas variable modifications were isotope labeling of lysine (+ 6.02 Da) and arginine (+ 10.01 Da) propionamide cysteine (+71) and oxidation of methionine (+16) with a maximal number of three modifications. A total of three missed cleavages by trypsin at lysine and arginine were allowed per peptide. All three search algorithms used a concatenated protein database, which was composed of forward and reverse sequences of the mouse RefSeq protein sequences (35,578 entries released on May 25, 2009 by National Center for Biotechnology Information, NCBI) plus common contaminant protein sequences *i.e.* porcine (Swiss-Prot P00761) and bovine (P00760) trypsin, and human keratin (P35908, Q01546, P04264, P12035, P08729, and P35527). The Sequest search was done on an eight-computer cluster, whereas the OMSSA and InsPecT searches were done on the National Institutes of Health Biowulf cluster (http://biowulf.nih.gov). For the Sequest search results from the LTQ spectra, the Xcorr scores were adjusted to specify a false discovery rate < 1% based on the target-decoy probability methods (27) whereas the following parameters remained constant: Xcorr rank = 1, SP rank = 1, and delta Cn > 0.08. For the Sequest search results from FT-ICR spectra, the filtering criteria included mass accuracy = 20 ppm. The InsPecT search results were filtered to a random match probability < 1% (p value < 0.01). The OMSSA search results were filtered to an false discovery rate < 1%. The search results from all three algorithms were pooled. To eliminate ambiguous identifications, at least two algorithms had to yield the same peptide identifications including modifications if a spectrum was interpreted by more than one algorithm. In addition, a new computational tool (*ProMatch* (28)) was used to identify and eliminate ambiguous protein identifications, *i.e.* tryptic peptides that are the same in two or more proteins (http://goo.gl/yhKa).

Peptides that matched to multiple proteins were included only if the matched proteins had at least one peptide that was a unique single match to the protein. Raw files, search results, and all spectra can be inspected by accessing the Peptidome database (accession number PSE132).

Quantification of peptides was performed using *QUIL*, an in-house software program (29). This program calculates light-to-heavy peptide abundance ratios on the basis of the areas under the relevant reconstructed elution profiles via numerical integration using the trapezoidal rule. All vasopressin/vehicle ratios were converted to base 2 logarithm ($\log_2$) values prior to further analysis. The median of the $\log_2$ values of all peptides identified for a given protein was used to infer the protein abundance change in one experiment. Only proteins with peptides quantified in all three experiments were used for statistical significance testing.

Multiple-Reaction Monitoring (MRM)—Cultured mpkCCD cells labeled with heavy or light amino acids as above were exposed to 0.1 nM dDAVP or vehicle for 5 days before their proteins were harvested, mixed at a 1:1 ratio, separated by one-dimensional SDS-PAGE, reduced, alkylated, trypsinized, and desalted before targeted MRM (multiple-reaction monitoring) proteomic analysis. MRM was carried out using a Tempo nano multi-dimensional liquid chromatography system coupled with a hybrid triple quadrupole linear ion trap mass

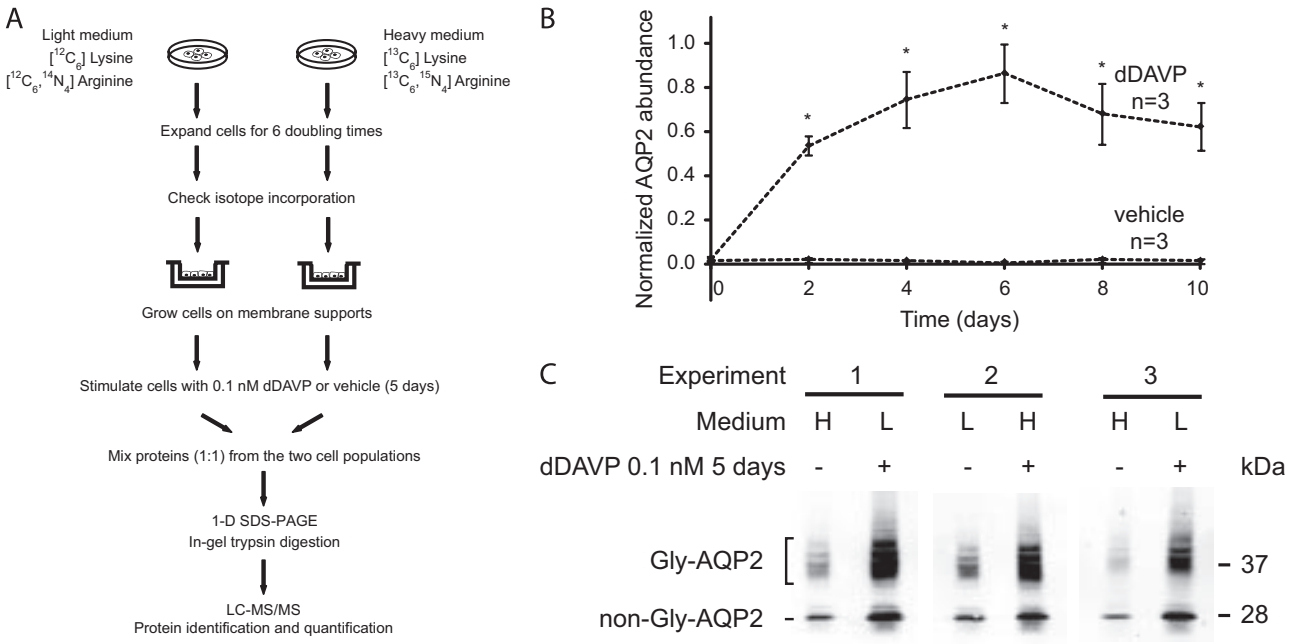

FIG. 1. **Quantitative SILAC LC-MS/MS protein mass spectrometry.** *A*, A flowchart of protocol for SILAC and LC-MS/MS. *B*, Time course of changes in aquaporin-2 (AQP2) protein abundance in mpkCCD cells in response to dDAVP. The mpkCCD cells were grown on membrane supports until confluence before they were exposed to 0.1 nM dDAVP or vehicle starting on day zero. Twenty μg protein samples collected at different time points were used for semiquantitative immunoblotting with an aquaporin-2 antibody. Values are mean ±S.E. Asterisks denote significant differences in aquaporin-2 abundances between dDAVP- and vehicle exposed cells for the same day ($p < 0.01$). Individual immunoblots are shown in the Supplemental Fig. S2. *C*, Steady-state aquaporin-2 protein abundance in mpkCCD cells used for LC-MS/MS quantification. The mpkCCD cells labeled with either heavy (H) or light (L) amino acids were grown on permeable supports until confluence before exposure to either 0.1 nM dDAVP or vehicle for 5 days. Proteins were extracted and used for immunoblotting with an aquaporin-2 antibody that detects both glycosylated (Gly-AQP2) and nonglycosylated aquaporin-2 (non-Gly-AQP2). 20 μg protein were loaded in each lane.

spectrometer (Q-Trap 4000, Applied Biosystems, Foster City, CA) equipped with a nanospray ion source (Applied Biosystems). Peptides were first loaded onto a trap cartridge (Zorbax 300SB-C18, 5 μm, 5 × 0.3 mm, Agilent Technologies) at a flow rate of 10 μl/min for 3 min. The trapped peptides were then fractionated with a reverse-phase Betabasic PicoFrit column (75 μm i.d. x 10 cm, 5 μm, 150Å, Thermo Fisher Scientific) using a linear gradient of 2%–60% ACN containing 0.1% FA. The duration of the gradient was 45 min at a flow rate of 0.25 μl/min followed by a wash with 80% ACN for 10 min. The eluted peptides from the PicoFrit column were sprayed into the mass spectrometer. The mass spectrometry was carried out with the following settings: spray voltage (2.4kV), ion transfer tube temperature (140 °C), curtain gas (10, arbitrary units), ion source gas (20, arbitrary units), and declustering potential (70, arbitrary units). The MRM acquisition was performed based on predetermined transition pairs for selected peptides (Supplemental Table S2). Fragmented product (Q3) masses were chosen on the basis of MS2 peak intensities from prior LTQ data-dependent experiments. The collision energy was adjusted automatically on the basis of mass and charge state of the precursor (Q1) mass, following manufacturer's rolling collision energy algorithm. Unit resolution was set for both Q1 and Q3. Data analysis was performed using *Analyst* software (version 1.4.2). For each protein, at least two peptides were selected for the MRM and at least two transitions per peptide were monitored. In addition, transitions for a particular peptide were required to be present at the same retention time for quantification.

Reverse Transcription and Polymerase Chain Reaction—Total RNA was extracted using the TriZOL reagent (15596–026) (Invitrogen) following the manufacturer's protocol. 0.5 μg total RNA were used for first strand cDNA synthesis using an oligo(dT) primer in a total volume of 20 μl (SuperScript™, Invitrogen) following the manufacturer's protocol. PCR product was generated from 0.5 μl of the first strand cDNA mixture using gene specific primers (Supplemental Table S3) and the ImmoMix (Bioline USA Inc., Randolph, MA). PCR was performed on a Peltier PCT-200 thermal cycler (MJ Research, Waltham, MA) with the following conditions: activation of the DNA polymerase at 95 °C for 7 min; 30 cycles of 94 °C for 30 s, 58 °C for 30 s, and 72 °C for 30 s; and a final extension at 72 °C for 10 min. PCR products were resolved with 1.6% agarose gel electrophoresis, stained with ethidium bromide, and visualized with the Gel Logic 100 imaging system (Eastman Kodak Co. Rochester, NY).

Real-time RT-PCR was performed with 200 ng of the first strand cDNA mixture using the 7900HT PCR system (Applied Biosystems) with the following conditions: 95 °C 10 min, 40 cycles of 95 °C 30 s, 55 °C 30 s, and 72 °C 30 s. At the end of the PCR reaction, dissociation curves of the PCR products were analyzed with the following condition 95 °C 15 s, 60 °C 15 s, and 95 °C 30 s. Real time PCR primers are in the Supplemental Table S3. Specificity of the gasdermin C isoform primers was confirmed by dissociation curve analysis of the PCR products (Supplemental Fig. S1) and by BLAST and BLAT analysis of the PCR product sequences.

Transcriptomic Analysis Using Oligonucleotide Microarrays—Total RNA was extracted using the TriZOL reagent (Invitrogen) as described above. Two micrograms of total RNA were used for oligonucleotide microarray analysis using Affymetrix GeneChip Mouse Genome 430 2.0 Arrays (NHLBI Gene Expression Core Facility). Full details are as described previously (30). Raw microarray data were analyzed with Affymetrix Gene Console software version 1.1 and normalized based

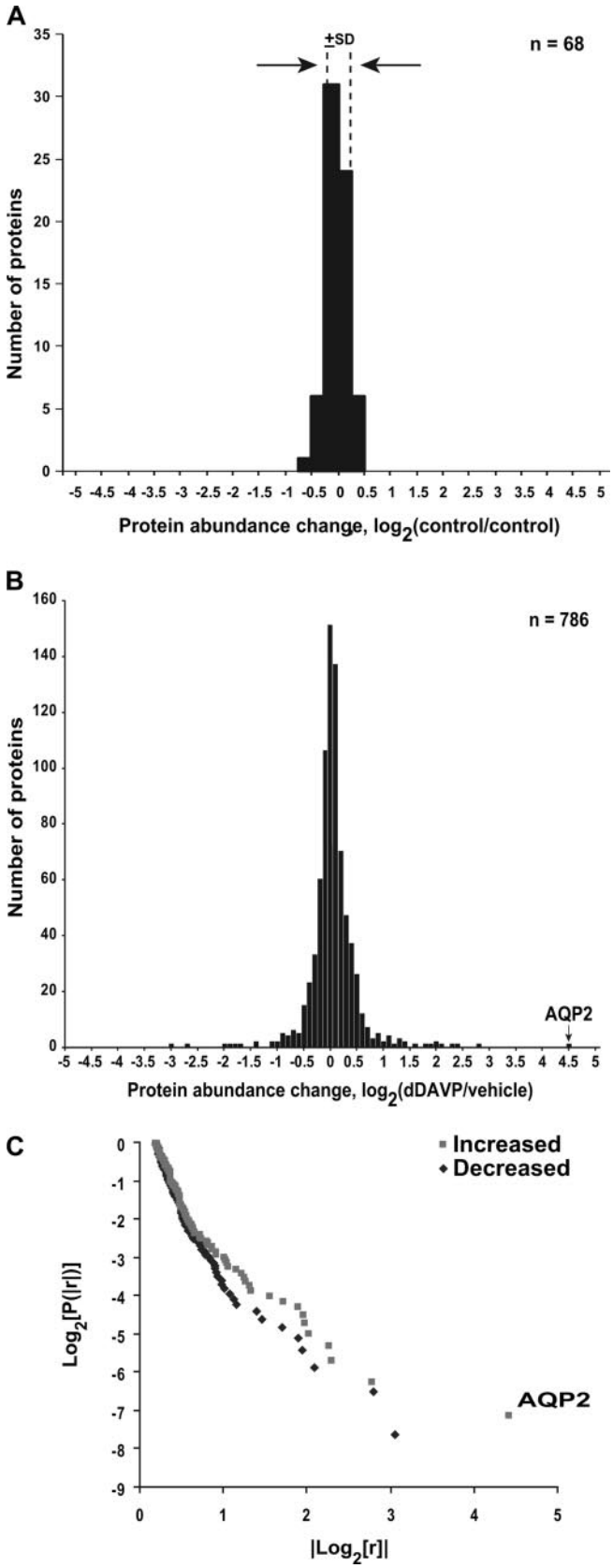

on the Robust Multichip Analysis algorithm. The normalized data were subjected to principal component analysis prior to statistical analysis and bioinformatics interpretation. Student's *t* test was used to test the significance of change.

RESULTS

Quantitative Proteomic Analysis of Long-Term Vasopressin Action—To identify proteins that change in abundance in mpkCCD clone 11 cells in response to the V2 receptor-selective vasopressin analog dDAVP, we carried out quantitative proteomic analysis using SILAC (*S*table *I*sotopic *L*abeling by *A*mino acids in *C*ell culture) coupled with tandem mass spectrometry (LC-MS/MS). Fig. 1*A* is a flowchart of the approach. Preliminary to the LC-MS/MS analysis, we carried out time course studies (Figs. 1*B*, Supplemental Fig. S2) to determine when, following the addition of dDAVP (0.1 nM), a maximal response was reached with respect to aquaporin-2 protein abundance. On the basis of these data, we chose 5 days for the period of dDAVP exposure in LC-MS/MS experiments. The cells used for LC-MS/MS analysis responded to 0.1 nM dDAVP with an increase in aquaporin-2 abundance in all three experimental pairs regardless of which stable-isotope label was included in the culture medium (Fig. 1*C*). In the quantitative proteomic analysis (Fig. 1*A*), three search algorithms (*InsPecT*, *OMSSA*, and *Sequest*) were used to assign specific peptide sequences to individual spectra, based on a mouse NCBI Reference Sequence (*RefSeq*) protein database. A target-decoy approach was used to filter search results to yield a false discovery rate $< 1\%$ (see *Experimental Procedures*).

A preliminary experiment was done to define the intrinsic variability of the SILAC-based quantification by comparing two nominally identical samples, labeled with the heavy and light amino acids, respectively. This experiment was carried out following the procedure described in Fig. 1*A* except that no vasopressin was added to either cell sample and the combined sample did not undergo one-dimensional SDS-PAGE prior to mass spectrometry. To quantify changes in protein abundance, we determined the areas under the curves of the reconstructed MS1 chromatograms for both labeled forms of each peptide using numerical integration based on the trapezoidal rule (31). Fig. 2A shows a histogram of the

Fig. 2. **SILAC LC-MS/MS protein quantification.** *A*, Variability of SILAC method. Distribution of protein abundance ratios for nominally identically treated cells (control *versus* control) except for labeling with SILAC light (L) and heavy (H) amino acids. The standard deviation of $\log_2$(L/H) values was $\pm$ 0.18 (dashed lines). Bin size = 0.25. *B*, Distribution of protein $\log_2$(D/C) values among all proteins quantified, where D is signal obtained in presence of dDAVP (5 day) and C is signal obtained in presence of vehicle. The value corresponding to aquaporin-2 (AQP2) abundance change is indicated. Bin size = 0.1. *C*, Log-log plot of cumulative probability *versus* absolute value of ratio for all mean values from Supplemental Table S4 in which log2(D/C) is greater than or equal to 0.2, showing "long-tailed distribution." AQP2 change is labeled.

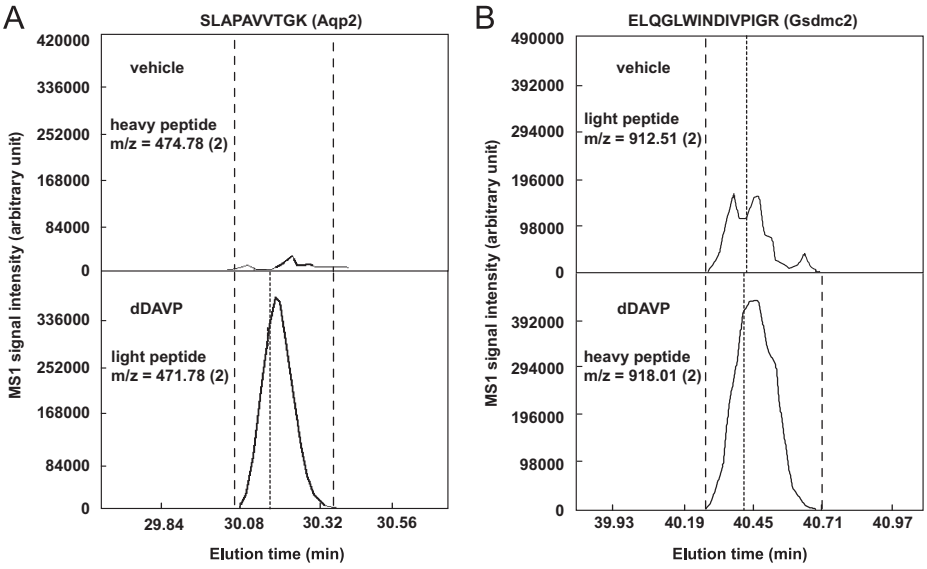

FIG. 3. **Typical reconstructed SILAC LC-MS/MS chromatograms for *A*, aquaporin-2 and *B*, gasdermin C2 peptides.** Examples of corresponding heavy- and light-labeled aquaporin-2 (*Aqp2*, NP_033829) and gasdermin C2 (*Gsdmc2*, NP_808580) peptides are shown. Quantification was carried out using the trapezoidal rule for numerical integration (QUIL program, see Experimental Procedures). Dashed lines define the range within which the peptide intensity was integrated. Dotted lines indicate the time point when a peptide sequence was identified. The *m/z* (charge) of the peptides are indicated. Similar results were obtained for all three sample pairs, despite alternating heavy and light labeling.

base-2 logarithm of the ratios calculated for each quantified protein. The standard deviation of $\log_2(\text{control}_1/\text{control}_2)$ was ± 0.18, corresponding to about a 13% increase or decrease.

In the experiments comparing the vasopressin analog dDAVP with vehicle, the spectra matched a total of 15,705 unique peptides (nonredundant sequences), which corresponded to 34,781 accession numbers and 5625 gene symbols in the mouse *RefSeq* protein database. To eliminate ambiguous protein identifications, peptide sequences with multiple gene symbols were included only if the matched protein had at least one peptide sequence that is a unique match to a single gene symbol (28). In this manner, a total of 2990 proteins were unambiguously identified, which we make publicly available via a new database, *viz*. the "NHLBI mpkCCD Proteome Database" (http://dir.nhlbi.nih.gov/papers/lkem/mpkccdproteome/). Raw spectra and search results are deposited in the Peptidome database, an NCBI Protein Mass Spectrometry Data Resource, with an accession number PSE132.

Most of the 2990 identified proteins were quantified in at least one experiment. All together, 768 proteins were quantified in all three experiments (Supplemental Table S4), allowing statistical testing of responses. Among these 768 proteins, most showed little or no change in abundance (Fig. 2*B*). Specifically, 598 proteins did not change significantly in response to dDAVP; 102 proteins were significantly increased in the dDAVP-treated cells whereas 86 proteins were significantly decreased. Fig. 2*C* shows the distribution of significantly changed abundance ratios for quantified proteins (plotted as the base-2 logarithm of the cumulative probability *versus* the absolute value of base 2 logarithm of the ratios). This figure shows a "log-tailed" non-Gaussian distribution, consisting of large numbers of proteins with small changes but with a few proteins with changes that are very, very large in magnitude. Lack of linearity of this plot argues against a classical power-law distribution, however. Note that, as shown in Fig. 2*B* and 2*C*, the increase in aquaporin-2 abundance exceeded increases seen for any other protein.

To provide an example of the quantification, Fig. 3 shows the reconstructed chromatograms for both labeled forms of selected aquaporin-2 (*Aqp2*) and gasdermin C2 (*Gsdmc2*) peptides. The areas under the reconstructed chromatograms of *Aqp2* and *Gsdmc2* peptides in the dDAVP-treated cells are greater than those in the vehicle-treated cells, indicating increases in *Aqp2* and *Gsdmc2* abundance in response to dDAVP. Similar results were seen in all three experimental sample pairs for these peptides as well as other *Aqp2* and *Gsdmc2* peptides.

Table I lists all 102 proteins that increased significantly in abundance in response to dDAVP. The increase in aquaporin-2 protein abundance was ~20-fold, in agreement with immunoblotting from the same experiment (Fig. 1*C*). Note the exceptional number of glutathione S-transferase proteins (*vide infra*) that were increased in abundance by dDAVP. Table II lists the 86 proteins that were significantly decreased in abundance in response to dDAVP.

Immunoblotting and Multiple Reaction Monitoring—To look more deeply at selected proteins quantified by SILAC LC-MS/MS, we used two approaches in freshly prepared samples: semiquantitative immunoblotting and multiple-reaction monitoring (MRM) LC-MS/MS. Immunoblotting with secondary antibodies conjugated to near-infrared fluorophors was used to quantify 16 proteins for which high quality primary antibodies were available: α-actinin-4 (*Actn4*), α-adducin isoform 3 (*Add1*), protein kinase A anchor protein 12 (*Akap12*), aquaporin-2 (*Aqp2*), macrophage-capping protein isoform 1 (*Capg*), carbonic anhydrase 2 (*Car2*), cathepsin D precursor (*Ctsd*), protein flightless-1 homolog (*Flii*), gelsolin precursor (*Gsn*), integrin β-1 precursor (*Itgb1*), LIM domain and actin-binding protein 1 isoform a (*Lima1*), microtubule-actin cross-

TABLE I

A list of proteins increased in abundance in mpkCCD cells in response to long-term (5 days) 0.1 nM dDAVP exposure. Results were calculated from all peptides quantified using SILAC in three LTQ-FT-ICR data-dependent experiments. Shown are $\log_2$ values of the mean of all peptide ratios (dDAVP: vehicle or D/V). All passed two-tailed *t*-test against $\log_2(1)$ ($p < 0.05$).

Protein name	Gene symbol	RefSeq no.	No. of peptides	$\log_2$(D/V) (Mean ± S.E.)
aquaporin 2	Aqp2	NP_033829	3	4.5 ± 0.6
MON2 homolog	Mon2	NP_700444	5	2.8 ± 0.4
hexose-6-phosphate dehydrogenase	H6pd	NP_775547	9	2.1 ± 0.2
A kinase (PRKA) anchor protein (gravin) 12	Akap12	NP_112462	24	2.0 ± 0.1
carnitine palmitoyltransferase 1A liver	Cpt1a	NP_038523	23	2.0 ± 0.1
UDP-N-acteylglucosamine pyrophosphorylase 1-like 1	Uap1l1	NP_001028465	8	1.9 ± 0.2
spectrin beta 3	Spnb3	NP_067262	53	1.4 ± 0.1
gasdermin C2	Gsdmc2	NP_808580	4	1.3 ± 0.4
isocitrate dehydrogenase 1 (NADP+), soluble	Idh1	NP_034627	20	1.3 ± 0.1
microtubule-actin crosslinking factor 1	Macf1	NP_033730	11	1.3 ± 0.1
glutathione S-transferase, theta 3	Gstt3	NP_598755	7	1.2 ± 0.3
glutathione S-transferase, theta 2	Gstt2	NP_034491	3	1.1 ± 0.2
MAL2 proteolipid protein	Mal2	NP_849251	1	1.1 ± 0.2
glutathione S-transferase, alpha 4	Gsta4	NP_034487	10	1.0 ± 0.1
dystonin isoform b	Dst	NP_604443	2	0.9 ± 0.3
cathepsin D	Ctsd	NP_034113	8	0.9 ± 0.2
aldo-keto reductase family 1, member C19	Akr1c19	NP_001013807	7	0.9 ± 0.1
indolethylamine N-methyltransferase	Inmt	NP_033375	7	0.8 ± 0.2
solute carrier family 25, member 13	Slc25a13	NP_056644	25	0.8 ± 0.1
legumain	Lgmn	NP_035305	4	0.8 ± 0.1
carbonic anhydrase II	Car2	NP_033931	9	0.7 ± 0.2
GDP-mannose 4,6-dehydratase	Gmds	NP_666153	5	0.7 ± 0.2
glutathione S-transferase, pi 1	Gstp1	NP_038569	13	0.7 ± 0.2
LIM domain and actin binding 1 isoform b	Lima1	NP_075550	2	0.7 ± 0.1
glutathione S-transferase mu 1	Gstm1	NP_034488	17	0.7 ± 0.1
abhydrolase domain containing 14b	Abhd14b	NP_083907	8	0.6 ± 0.2
ATP citrate lyase	Acly	NP_598798	25	0.6 ± 0.1
spectrin alpha 2	Spna2	NP_001070022	124	0.6 ± 0.1
caldesmon 1	Cald1	NP_663550	6	0.6 ± 0.1
ciliary rootlet coiled-coil isoform 1	Crocc	NP_742120	1	0.6 ± 0.1
transglutaminase 2, C polypeptide	Tgm2	NP_033399	7	0.6 ± 0.1
ubiquilin 2	Ubqln2	NP_061268	2	0.6 ± 0.1
F-box protein 18	Fbxo18	NP_056607	1	0.5 ± 0.2
SMC hinge domain containing 1	Smchd1	NP_083163	6	0.5 ± 0.2
RalGDS-like protein 3	Rgl3	NP_076111	9	0.5 ± 0.2
hydroxyacyl-Coenzyme A dehydrogenase type II	Hsd17b10	NP_058043	12	0.5 ± 0.2
NADH dehydrogenase (ubiquinone) Fe-S protein 1	Ndufs1	NP_663493	7	0.5 ± 0.1
flightless I homolog	Flii	NP_071292	12	0.5 ± 0.1
calpastatin	Cast	NP_033947	4	0.5 ± 0.1
radixin isoform a	Rdx	NP_033067	18	0.5 ± 0.1
moesin	Msn	NP_034963	21	0.5 ± 0.1
cytochrome b5 type B precursor	Cyb5b	NP_079834	5	0.5 ± 0.1
solute carrier family 25, member 12	Slc25a12	NP_766024	10	0.5 ± 0.1
glutamate dehydrogenase 1	Glud1	NP_032159	9	0.5 ± 0.1
alanyl-tRNA synthetase	Aars	NP_666329	22	0.5 ± 0.1
brain abundant, membrane attached signal protein 1	Basp1	NP_081671	8	0.5 ± 0.1
osteoclast stimulating factor 1	Ostf1	NP_059071	3	0.4 ± 0.2
fatty acid synthase	Fasn	NP_032014	71	0.4 ± 0.2
tight junction protein 2	Tjp2	NP_035727	18	0.4 ± 0.2
N-acylsphingosine amidohydrolase 1	Asah1	NP_062708	10	0.4 ± 0.1
cytochrome P450 reductase	Por	NP_032924	23	0.4 ± 0.1
actinin, alpha 1	Actn1	NP_598917	49	0.4 ± 0.1
keratin complex 2, basic, gene 17	Krt2	NP_034798	9	0.4 ± 0.1
transmembrane protein 33 isoform 2	Tmem33	NP_084384	3	0.4 ± 0.1
peroxiredoxin 5 precursor	Prdx5	NP_036151	12	0.4 ± 0.1
actinin alpha 4	Actn4	NP_068695	37	0.4 ± 0.1
keratin 18	Krt18	NP_034794	29	0.4 ± 0.1
p21-activated kinase 3	Pak3	NP_032804	6	0.4 ± 0.1

TABLE I—*continued*

Protein name	Gene symbol	RefSeq no.	No. of peptides	Log_2(D/V) (Mean ± S.E.)
keratin 6A	Krt6a	NP_032502	13	0.4 ± 0.1
delta-aminolevulinic acid dehydratase	Alad	NP_032551	11	0.4 ± 0.1
plastin 3 precursor	Pls3	NP_663604	12	0.4 ± 0.1
CNDP dipeptidase 2	Cndp2	NP_075638	13	0.4 ± 0.1
pyruvate carboxylase	Pcx	NP_032823	12	0.4 ± 0.1
nicotinamide phosphoribosyltransferase	Nampt	NP_067499	14	0.4 ± 0.1
clathrin, heavy polypeptide (Hc)	Cltc	NP_001003908	76	0.3 ± 0.1
pyruvate dehydrogenase (lipoamide) beta	Pdhb	NP_077183	5	0.3 ± 0.1
electron transferring flavoprotein, alpha polypeptide	Etfa	NP_663590	13	0.3 ± 0.1
family with sequence similarity 129, member A	Fam129a	NP_071301	20	0.3 ± 0.1
superoxide dismutase 2, mitochondrial	Sod2	NP_038699	4	0.3 ± 0.1
keratin 6L	Krt79	NP_666175	9	0.3 ± 0.1
spectrin beta 2 isoform 1	Spnb2	NP_787030	62	0.3 ± 0.1
tight junction protein 1	Tjp1	NP_033412	10	0.3 ± 0.1
keratin 5	Krt5	NP_081287	17	0.3 ± 0.1
phosphogluconate dehydrogenase	Pgd	NP_001074743	10	0.3 ± 0.1
N-myc downstream regulated 1	Ndrg1	NP_032707	9	0.3 ± 0.1
p21-activated kinase 2	Pak2	NP_796300	14	0.3 ± 0.1
SWI/SNF-related matrix-associated actin-dependent regulator of chromatin c2 isoform 3	Smarcc2	NP_937803	10	0.3 ± 0.1
seryl-tRNA synthetase	Sars	NP_035449	15	0.3 ± 0.1
oxidation resistance 1 isoform A	Oxr1	NP_570955	11	0.3 ± 0.1
keratin complex 2, basic, gene 8	Krt8	NP_112447	40	0.3 ± 0.1
Wiskott-Aldrich syndrome-like	Wasl	NP_082735	5	0.3 ± 0.1
SKI interacting protein	Snw1	NP_079783	3	0.2 ± 0.1
drebrin-like isoform 2	Dbnl	NP_038838	4	0.2 ± 0.1
neural precursor cell expressed, developmentally down-regulated gene 4	Nedd4	NP_035020	17	0.2 ± 0.1
heat shock protein 9	Hspa9	NP_034611	29	0.2 ± 0.1
periplakin	Ppl	NP_032935	74	0.2 ± 0.1
isoleucine tRNA synthetase	Iars	NP_742012	22	0.2 ± 0.1
chaperonin containing Tcp1, subunit 5 (epsilon)	Cct5	NP_031663	15	0.2 ± 0.1
dipeptidyl peptidase III	Dpp3	NP_598564	14	0.2 ± 0.1
valosin containing protein	Vcp	NP_033529	24	0.2 ± 0.1
phospholipase C beta 3	Plcb3	NP_032900	23	0.2 ± 0.1
aconitase 2, mitochondrial	Aco2	NP_542364	35	0.2 ± 0.1
chaperonin subunit 2 (beta)	Cct2	NP_031662	13	0.2 ± 0.1
coatomer protein complex, subunit gamma isoform 1	Copg	NP_059505	8	0.2 ± 0.1
ubiquitin-activating enzyme E1 isoform 1	Uba1	NP_033483	14	0.2 ± 0.1
ubiquinol cytochrome c reductase core protein 2	Uqcrc2	NP_080175	7	0.1 ± 0.1
B-cell receptor-associated protein 37	Phb2	NP_031557	12	0.1 ± 0.1
heat shock protein 4	Hspa4	NP_032326	30	0.1 ± 0.1
keratin 19	Krt19	NP_032497	30	0.1 ± 0.1
peroxiredoxin 4	Prdx4	NP_058044	3	0.1 ± 0.1
voltage-dependent anion channel 2	Vdac2	NP_035825	10	0.1 ± 0.1
high density lipoprotein binding protein	Hdlbp	NP_598569	26	0.1 ± 0.1

linking factor 1 (*Macf1*), protein MAL2 (*Mal2*), Na/H exchange regulatory cofactor NHERF1 (*Slc9a3r1*), spectrin β-chain, brain 1 isoform 2 (*Spnb2*), and protein-glutamine γ-glutamyltransferase 2 (*Tgm2*). Supplemental Fig. S3 shows the immunoblotting results. Fig. 4 compares the immunoblotting results with the SILAC LC-MS/MS results. The immunoblotting results are consistent with the SILAC LC-MS/MS results with regard to direction of change for 13 out of 16 proteins in response to dDAVP exposure for 5 days.

MRM LC-MS/MS combined with SILAC was used to verify the LC-MS/MS quantification results for 9 selected proteins (Table III), including three that were also quantified by immunoblotting, viz. Aqp2, Nherf1, and Mal2, and six for which adequate antibodies were unavailable. All 9 of these targeted proteins are potentially relevant to vasopressin signaling (Table III) and are all relatively abundant proteins as is necessary because of limitations in the sensitivity of the mass spectrometer used for the experiments (ABI Q-Trap 4000). (We attempted to quantify all of the SILAC "hits" by MRM, but were not able to obtain reliable quantifications for the majority of targeted proteins, and this was because the mass resolution and signal-to-noise ratio were not suf-

TABLE II

A list of proteins decreased in abundance in mpkCCD cells in response to long-term (5 days) 0.1 nM dDAVP exposure. Results were calculated from all peptides quantified using SILAC in three LTQ-FT-ICR data-dependent experiments. Shown are $\log_2$ values of the mean of all peptide ratios (dDAVP: vehicle or D/V). All passed two-tailed *t*-test against $\log_2(1)$ ($p < 0.05$).

Protein name	Gene symbol	RefSeq no.	No. of peptides	$\log_2$(D/V) (Mean ± S.E.)
mediator of DNA damage checkpoint 1	Mdc1	NP_001010833	3	−1.5 ± 0.1
DNA methyltransferase (cytosine-5) 1	Dnmt1	NP_034196	16	−1.2 ± 0.3
myosin, light polypeptide kinase	Mylk	NP_647461	13	−1.1 ± 0.3
nucleoporin 210	Nup210	NP_061285	11	−1.0 ± 0.3
pinin	Pnn	NP_032917	5	−0.9 ± 0.2
gelsolin	Gsn	NP_666232	22	−0.9 ± 0.1
basal cell adhesion molecule	Bcam	NP_065232	4	−0.9 ± 0.1
FK506 binding protein 5	Fkbp5	NP_034350	1	−0.8 ± 0.2
PREDICTED: desmoplakin isoform 2	Dsp	XP_901443	18	−0.8 ± 0.2
glycerol-3-phosphate dehydrogenase 1 (soluble)	Gpd1	NP_034401	10	−0.7 ± 0.1
D6Wsu176e protein	Fam3c	NP_613053	3	−0.7 ± 0.1
myristoylated alanine rich protein kinase C substrate	Marcks	NP_032564	6	−0.7 ± 0.1
ladinin	Lad1	NP_598425	7	−0.6 ± 0.2
minichromosome maintenance deficient 2 mitotin	Mcm2	NP_032590	32	−0.6 ± 0.2
adenine phosphoribosyltransferase	Aprt	NP_033828	6	−0.6 ± 0.1
cadherin 16	Cdh16	NP_031689	12	−0.6 ± 0.1
PDZ and LIM domain 5 isoform ENH1	Pdlim5	NP_062782	9	−0.6 ± 0.1
Rho, GDP dissociation inhibitor (GDI) beta	Arhgdib	NP_031512	4	−0.6 ± 0.1
H1 histone family, member 0	H1f0	NP_032223	4	−0.6 ± 0.1
cystatin B	Cstb	NP_031819	4	−0.5 ± 0.2
membrane bound C2 domain containing protein	Mbc2	NP_035973	2	−0.5 ± 0.2
minichromosome maintenance deficient 5, cell division cycle 46	Mcm5	NP_032592	27	−0.5 ± 0.2
guanine monophosphate synthetase	Gmps	NP_001028472	9	−0.5 ± 0.2
synaptotagmin binding, cytoplasmic RNA interacting protein isoform 2	Syncrip	NP_062770	10	−0.5 ± 0.1
minichromosome maintenance complex component 6	Mcm6	NP_032593	20	−0.5 ± 0.1
activity-dependent neuroprotective protein	Adnp	NP_033758	3	−0.5 ± 0.1
suppressor of Ty 16 homolog	Supt16h	NP_291096	14	−0.5 ± 0.1
annexin A6 isoform a	Anxa6	NP_038500	38	−0.5 ± 0.1
estradiol 17-beta-dehydrogenase 11	Hsd17b11	NP_444492	5	−0.5 ± 0.1
thymopoietin isoform delta	Tmpo	NP_001073599	15	−0.5 ± 0.1
sterile alpha motif domain containing 9-like	Samd9l	NP_034286	29	−0.5 ± 0.1
minichromosome maintenance complex component 7	Mcm7	NP_032594	22	−0.5 ± 0.1
integrin beta 1 (fibronectin receptor beta)	Itgb1	NP_034708	12	−0.4 ± 0.1
isocitrate dehydrogenase 2 (NADP+), mitochondrial	Idh2	NP_766599	12	−0.4 ± 0.1
filamin B, beta	Flnb	NP_598841	92	−0.4 ± 0.1
activator of heat shock 90kDa protein ATPase homolog 1	Ahsa1	NP_666148	3	−0.4 ± 0.1
integrin alpha 3	Itga3	NP_038593	9	−0.4 ± 0.1
apoptotic chromatin condensation inducer 1 isoform 2	Acin1	NP_075679	5	−0.4 ± 0.1
transcription elongation factor A (SII) 1 isoform 2	Tcea1	NP_035671	2	−0.4 ± 0.1
glutathione S-transferase, alpha 3	Gsta3	NP_034486	8	−0.4 ± 0.1
annexin A2	Anxa2	NP_031611	24	−0.4 ± 0.1
dihydropyrimidinase-like 2	Dpysl2	NP_034085	13	−0.4 ± 0.1
vinculin	Vcl	NP_033528	42	−0.4 ± 0.1
filamin C, gamma	Flnc	NP_001074654	16	−0.4 ± 0.1
unc-84 homolog B	Unc84b	NP_919323	2	−0.4 ± 0.1
glyoxalase 1	Glo1	NP_079650	5	−0.3 ± 0.1
heterogeneous nuclear ribonucleoprotein U	Hnrnpu	NP_058085	28	−0.3 ± 0.1
KH-type splicing regulatory protein	Khsrp	NP_034743	18	−0.3 ± 0.1
protein disulfide isomerase A6	Pdia6	NP_082235	8	−0.3 ± 0.1
cytochrome c oxidase, subunit Va	Cox5a	NP_031773	7	−0.3 ± 0.1
splicing factor 3a, subunit 2	Sf3a2	NP_038679	2	−0.3 ± 0.1
chromodomain helicase DNA binding protein 4	Chd4	NP_666091	49	−0.3 ± 0.1
arsenate resistance protein 2 isoform 1	Srrt	NP_113582	10	−0.3 ± 0.1
U5 snRNP-specific protein, 200 kDa	Snrnp200	NP_796188	46	−0.3 ± 0.1
protein disulfide isomerase A4	Pdia4	NP_033917	22	−0.3 ± 0.1

TABLE II—*continued*

Protein name	Gene symbol	RefSeq no.	No. of peptides	Log_2(D/V) (Mean ± S.E.)
cytochrome c oxidase subunit IV isoform 1	Cox4i1	NP_034071	5	−0.3 ± 0.1
importin 5	Ipo5	NP_076068	6	−0.3 ± 0.1
adaptor protein complex AP-1, gamma 1 subunit	Ap1g1	NP_033807	8	−0.3 ± 0.1
tumor rejection antigen gp96	Hsp90b1	NP_035761	31	−0.3 ± 0.1
serine hydroxymethyltransferase 2 (mitochondrial)	Shmt2	NP_082506	12	−0.3 ± 0.1
apoptosis-inducing factor, mitochondrion-associated 1	Aifm1	NP_036149	7	−0.3 ± 0.1
LPS-responsive beige-like anchor isoform alpha	Lrba	NP_109620	68	−0.3 ± 0.1
L-3-hydroxyacyl-Coenzyme A dehydrogenase	Hadh	NP_032238	11	−0.3 ± 0.1
integral membrane protein 1	Stt3a	NP_032434	3	−0.3 ± 0.1
alpha thalassemia/mental retardation syndrome X-linked homolog	Atrx	NP_033556	1	−0.3 ± 0.1
FK506 binding protein 52	Fkbp4	NP_034349	10	−0.3 ± 0.1
peptidylprolyl isomerase B	Ppib	NP_035279	14	−0.3 ± 0.1
NADH dehydrogenase ubiquinone flavoprotein 2 precursor	Ndufv2	NP_082664	1	−0.3 ± 0.1
protease (prosome, macropain) 26S subunit, ATPase 5	Psmc5	NP_032976	2	−0.2 ± 0.1
nuclear pore complex-associated protein Tpr	Tpr	NP_598541	29	−0.2 ± 0.1
splicing factor, arginine/serine-rich 7	Sfrs7	NP_666195	5	−0.2 ± 0.1
gelsolin-like capping protein isoform 1	Capg	NP_031625	11	−0.2 ± 0.1
karyopherin (importin) beta 1	Kpnb1	NP_032405	28	−0.2 ± 0.1
small nuclear ribonucleoprotein E	Snrpe	NP_033253	1	−0.2 ± 0.1
nucleolin	Ncl	NP_035010	21	−0.2 ± 0.1
DEAH (Asp-Glu-Ala-His) box polypeptide 9	Dhx9	NP_031868	35	−0.2 ± 0.1
voltage-dependent anion channel 3	Vdac3	NP_035826	7	−0.2 ± 0.1
HLA-B-associated transcript 3	Bat3	NP_476512	7	−0.2 ± 0.1
heterogeneous nuclear ribonucleoprotein A1 isoform a	Hnrnpa1	NP_034577	16	−0.2 ± 0.1
SEC22 vesicle trafficking protein-like 1	Sec22b	NP_035472	5	−0.2 ± 0.1
nucleoside diphosphate kinase B	Nme2	NP_032731	9	−0.2 ± 0.1
splicing factor 3b, subunit 3	Sf3b3	NP_598714	26	−0.2 ± 0.1
pre-mRNA processing factor 8	Prpf8	NP_619600	39	−0.1 ± 0.1
PREDICTED: similar to Heat shock protein 1 (chaperonin)	Hspd1	XP_484008	25	−0.1 ± 0.1
ribosomal protein L18	Rpl18	NP_033103	6	−0.1 ± 0.1
voltage-dependent anion channel 1	Vdac1	NP_035824	14	−0.1 ± 0.1

ficient to have confidence in the correct identification of specific transitions. In general, MRM quantifications worked well but only for the relatively abundant proteins.) The MRM experiments used SILAC-labeled peptides. The transitions for both the light and heavy forms of selected peptides were monitored. As summarized in Table III and Supplemental Fig. S4, in general the MRM LC-MS/MS method yielded quantification results consistent with the nontargeted SILAC LC-MS/MS method.

Quantitative Transcriptomic Analysis of Long-Term Vasopressin Action—To address whether changes in protein abundance measured by SILAC LC-MS/MS are generally because of corresponding changes in mRNA levels, we carried out oligonucleotide microarray experiments (Affymetrix) in mpkCCD cells treated in the same manner (0.1 nM dDAVP or vehicle for 5 days). Fig. 5A shows the results of RT-PCR measurements of aquaporin-2 mRNA, confirming the efficacy of dDAVP in eliciting a physiological response.

Total RNA from these experiments was used for global measurements of mRNA abundances (Affymetrix, Mouse Genome 430 2.0 Arrays). A total of 15,537 nonredundant mRNA species were quantified (Supplemental Table S5). A histogram of all changes is shown in Fig. 5*B*. Most of the measured transcripts did not change significantly in abundance in response to dDAVP (Supplemental Table S5). Table IV lists the 42 mRNA species that increased in abundance by more than 50% (*i.e.* $\log_2$(dDAVP/vehicle) > 0.585). Table V lists the three mRNA species that decreased in abundance to $\log_2$(dDAVP/vehicle) < -0.585, *i.e.* by greater than one-third. To further evaluate the transcript measurements by the Affymetrix microarray, real time RT-PCR experiments were performed. Fig. 6 confirms the general correlation between array measurements and PCR measurements. All raw data from the microarray experiments can be retrieved from NCBI Gene Expression Omnibus with an accession number GSE19938. Summarized data, including official gene symbols of all quantified transcripts, are in the Supplemental Table S5.

Of the 786 proteins quantified in all three experiments by nontargeted SILAC LC-MS/MS, the microarray experiments successfully quantified mRNA abundance levels for 766 of them in three independent experiments. Among the 188 proteins that showed significant changes in abundance, 186 of them had corresponding transcript abundance quantified. Among them, only 22% (40/186) exhibited statistically significant changes in the abundance of corresponding

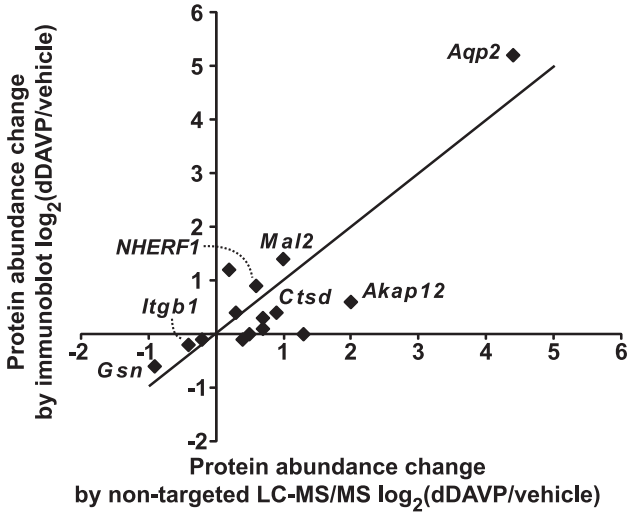

Protein Name	Gene Symbol	Mean SILAC	Mean IB
aquaporin-2	*Aqp2*	4.5*	5.2*
A-kinase anchor protein 12	*Akap12*	2.0*	0.6*
microtubule-actin cross-linking factor 1	*Macf1*	1.3*	0.0
protein MAL2	*Mal2*	1.1*	1.4*
cathepsin D precursor	*Ctsd*	0.9*	0.4*
carbonic anhydrase 2	*Car2*	0.7*	0.3
LIM domain and actin-binding protein 1 isoform a	*Lima1*	0.7*	0.1
protein-glutamine gamma-glutamyltransferase 2	*Tgm2*	0.6*	0.2
alpha-adducin isoform 3	*Add1*	0.5	1.2*
Na(+)/H(+) exchange regulatory cofactor NHERF1	*Slc9a3r1*	0.5	0.9*
protein flightless-1 homolog	*Flii*	0.5*	0.0
alpha-actinin-4	*Actn4*	0.4*	-0.1
spectrin beta chain, brain 1 isoform 2	*Spnb2*	0.3*	0.4
capping protein (actin filament), isoform 1	*Capg*	-0.2*	-0.1
integrin beta-1 precursor	*Itgb1*	-0.4*	-0.2
gelsolin precursor	*Gsn*	-0.9*	-0.6

FIG. 4. **Comparison of SILAC LC-MS/MS quantification with semiquantitative immunoblotting.** Immunoblots are shown in the Supplemental Fig. S3. Log_2 values of the protein abundance ratios for paired dDAVP- and vehicle-exposed cells are shown on the right [mean ± S.E., $^{*}p < 0.05$ *versus* $log_2(1)$]. IB, immunoblot. The RefSeq accession numbers are: *Actn4*, NP_068695; *Add1*, NP_001095914; *Akap12*, NP_112462; *Aqp2*, NP_033829; *Capg*, NP_031625; *Car2*, NP_033931; *Ctsd*, NP_034113; *Flii*, NP_071292; *Gsn*, NP_666232; *Itgb1*, NP_034708; *Lima1*, NP_075550; *Macf1*, NP_033730; *Mal2*, NP_849251; *Nherf1*, NP_036160; *Spnb2*, NP_787030; and *Tgm2*, NP_033399.

mRNAs. Given the fact that the quantitative comparisons using SILAC LC-MS/MS are done in a single combined sample in which both vasopressin and control states are analyzed simultaneously for multiple peptides, it is likely that the precision of protein abundance comparisons is greater than transcriptomic comparisons that involve two parallel Affymetrix array hybridizations. Thus, it could be argued that the failure to detect changes in mRNA levels for some of the proteins showing changes in abundance could be because of a lower sensitivity for the Affymetrix-based mRNA quantification (*i.e.* lower statistical power). This possibility was ruled out by the data shown in Fig. 7*A*, plotting the statistical power when testing for percent mRNA changes equivalent to the measured protein abundance changes. As anticipated, several of the mRNA abundance comparisons for proteins showing small, but significant changes in protein abundance, had low statistical power. However, if comparisons were restricted to those with statistical power greater than 0.8, only 26% (40/154) showed significant changes in mRNA levels (Fig. 7*B*). These results suggest that post-transcriptional mechanisms account for the changes in protein abundances for a large fraction (~74% in these experiments) of protein species exhibiting altered abundances in response to vasopressin. To address whether this conclusion would be different for proteins that underwent large *versus* small fractional changes in abundance, we have plotted the percent of proteins with associated changes in transcript levels as a function of the absolute value of log_2(dDAVP/control) in Fig. 7*C*. As can be seen, only approximately two-thirds of proteins that undergo a change in the absolute value of log_2(dDAVP/control) greater than 1.0 (doubling or halving), have corresponding changes in transcript levels. Thus, even among proteins undergoing the largest changes, a substantial fraction do so without detectable mRNA changes.

As shown in Fig. 8, there is a difference in the degree of protein-mRNA correspondence between up-regulated and down-regulated proteins. (Fig. 8 includes only genes whose mRNA measurements had a statistical power greater than 0.8.) Of the 64 proteins that showed a statistically significant decrease in abundance in response to dDAVP, only 6% of them (4/64) had corresponding decreases in mRNA abundance, whereas 37% (33/90) of the proteins that increased in abundance in response to dDAVP had associated increases in mRNA abundance.

Fig. 9 displays the 40 genes for which protein abundance and mRNA abundance both underwent significant changes. *Aqp2* and *Gsdmc2* were the only two genes that showed correlated increases in both mRNA and protein abundances greater than 100% in response to dDAVP, indicating a high degree of selectivity for vasopressin-mediated transcriptional responses. Real-time RT-PCR experiments confirmed increases in *Gsdmc2* mRNA abundances in response to 0.1 nM dDAVP for 5 days (Fig. 6).

TABLE III

Comparison of protein abundance quantification in targeted LC-MS/MS experiments (MRM) versus data-dependent LC-MS/MS experiments. Changes in protein abundance in response to long-term (5 days) dDAVP (D) versus vehicle (V). Values are Mean ± S.E. of $\log_2$ (D/V).

Protein name (gene symbol, Refseq)	Annotation (from Swiss-Prot)	Targeted LC-MS/MS $\log_2$ (D/V)	Non-targeted LC-MS/MS $\log_2$ (D/V)
Aquaporin 2 (Aqp2, NP_033829)	Vasopressin-regulated water-specific channel that provides the plasma membranes of renal collecting duct with high permeability to water, thereby permitting water to move in the direction of an osmotic gradient.	3.3 ± 0.4*	4.4 ± 0.5*
MON2 homolog (Mon2, NP_700444)	May be required for traffic between late Golgi and early endosomes.	3.6 ± 1.1*	2.8 ± 0.3*
MAL2 proteolipid protein (Mal2, NP_849251)	Member of the machinery of polarized transport. Required for the indirect transcytotic route at the step of the egress of the transcytosing cargo from perinuclear endosomes in order for it to travel to the apical surface via a raft-dependent pathway.	0.7 ± 0.1	1.0 ± 0.2*
Dystonin isoform a/b (Dst, NP_598594; NP_604443)	Cytoskeletal linker protein. Anchors keratin-containing intermediate filaments to the inner plaque of hemi-desmosomes. The proteins may self-aggregate to form filaments or a two-dimensional mesh.	0.1 ± 0.1	0.9 ± 0.2*
Sodium/hydrogen exchanger regulatory factor 1, NHERF1 (Slc9a3r1, NP_036160)	Scaffold protein that connects plasma membrane proteins with members of the ezrin/moesin/radixin family and thereby helps to link them to the actin cytoskeleton and to regulate their surface expression. Necessary for cAMP-mediated phosphorylation and inhibition of SLC9A3. May enhance Wnt signaling.	0.7 ± 0.4*	0.5 ± 0.2
Lysosomal membrane glycoprotein 2 isoform 2 (Lamp2, NP_034815)	May function in protection of the lysosomal membrane from autodigestion, maintenance of the acidic environment of the lysosome, adhesion when expressed on the cell surface (plasma membrane), and inter- and intracellular signal transduction. Protects cells from the toxic effects of methylating mutagens.	0.4 ± 0.5	0.5 ± 0.5
RAB7 (Rab7, NP_033031)	Involved in late endocytic transport. Contributes to the maturation of phagosomes (acidification).	0.2 ± 0.1	0.1 ± 0.1
Na^+/K^+-ATPase a1 subunit (Atp1a1, NP_659149)	Catalytic component of the active enzyme that catalyzes the hydrolysis of ATP coupled with the exchange of sodium and potassium ions across the plasma membrane. This action creates the electrochemical gradient of sodium and potassium ions, providing the energy for active transport of various nutrients.	0.3 ± 0.2	−0.2 ± 0.1
Tight junction protein 1 or ZO-1 (Tjp1, NP_033412)	The N-terminal [portion] may be involved in transducing a signal required for tight junction assembly, while the C-terminal [portion] may have specific properties of tight junctions. The alpha domain might be involved in stabilizing junctions.	−0.1 ± 0.0	−0.2 ± 0.0*

* Statistically significant by two-tailed t-test against $\log_2(1)$ ($p < 0.05$).

Analysis of Biological Processes Related to Vasopressin-Regulated Proteins—As noted above, 188 proteins of the 786 proteins quantified in all three experiments were found to change significantly in abundance in mpkCCD cells in response to the vasopressin analog dDAVP. We used the DAVID bioinformatic tool (*Database for Annotation, Visualization and Integrated Discovery*, NIAID, http://david.abcc.ncifcrf.gov/(32)) to ask whether the regulated proteins are associated with specific biological processes or molecular functions. For this, we compared the regulated protein list with the list of all genes expressed in mpkCCD cells (mpkCCD Transcriptome Database, http://dir.nhlbi.nih.gov/papers/lkem/mpkccdtr) to determine *Gene Ontology (GO) Biological Processes* or *Molecular Functions* that are statis-

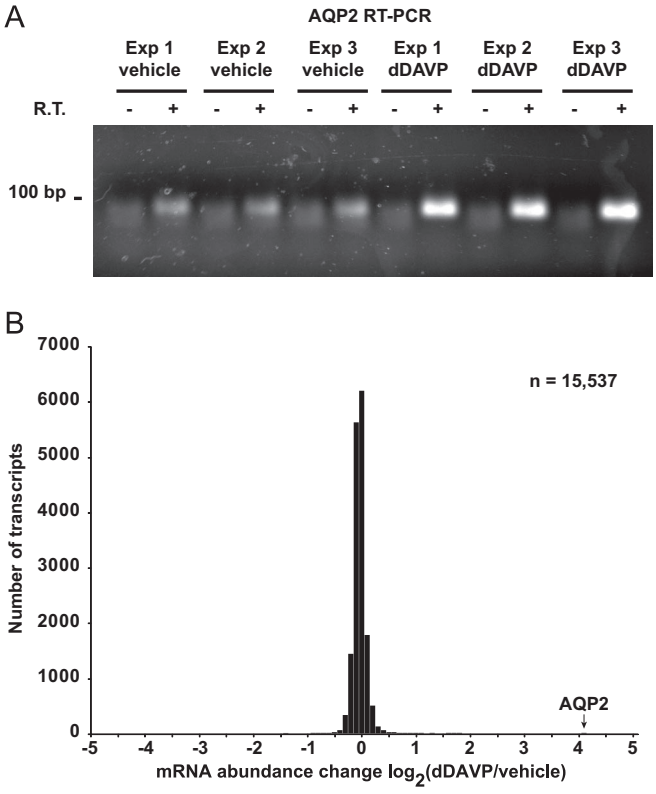

FIG. 5. **Transcript changes in mpkCCD cells in response to vasopressin analog dDAVP.** *A*, Aquaporin-2 mRNA abundance changes in mpkCCD cells in response to dDAVP. Polarized mpkCCD cells grown on membrane supports were exposed to dDAVP or vehicle for 5 days. Total RNA was extracted and used for reverse transcription and polymerase chain reaction analysis (RT-PCR): 0.5 μg of total RNA per sample; 30 cycles of PCR. -, no RT reaction control; V, vehicle; D, 0.1 nM dDAVP. *B*, Distribution of mRNA abundance changes in response to dDAVP among all transcripts quantified. The bar corresponding to aquaporin-2 response is indicated. The results were obtained from Affymetrix GeneChip Mouse Genome 430 2.0 Arrays.

tically significantly enriched in the regulated proteins. As a control, we also analyzed the list of 598 nonregulated proteins *versus* the list of all expressed genes. Most of the GO Biological Processes that were significantly enriched in the regulated protein group ($p < 0.05$, Fisher exact test) were related to actin cytoskeletal organization (Fig. 10, top). The control dataset did not identify any of the same GO Biological Process terms (Fig. 10, bottom) and instead most of the terms significantly enriched in the unregulated protein data set are related to energy metabolism and protein synthesis. Table VI lists the regulated proteins in the "actin cytoskeleton organization and biogenesis" GO Biological Processes category. Among the 13 proteins in this group, three are significantly decreased in abundance and 10 are significantly increased. Among the three that were decreased were two gelsolin-like proteins including gelsolin itself and gelsolin-like capping protein G. These two proteins are involved in severing F-actin filaments and capping the barbed ends. Among the 10 proteins up-regulated in the "actin cytoskeleton organization and biogenesis" GO category, five are involved in cross linking or bundling of F-actin, namely two isoforms of α-actinin and three isoforms of spectrin. The former is involved in organization of F-actin into stress fibers, whereas the later is an actin-binding protein that organizes short actin filaments into a two-dimensional web abutting the plasma membrane. This network is instrumental in maintaining plasma membrane shape in part by binding to the cytoplasmic tails of integral membrane proteins. The coordinate up-regulation of these α-actinin and spectrin proteins by vasopressin is therefore compatible with a role for vasopressin in regulating F-actin crosslinking with itself and other proteins. Also up-regulated was drebrin-like protein (an actin-binding protein thought to be involved in regulation of endocytosis through interactions with dynamin), Wiskott-Aldrich syndrome-like protein (which increases actin polymerization by activating the Arp2/3 protein complex), radixin (an ERM protein that links F-actin to integral membrane proteins), and cytokeratin 19 (an intermediate filament protein that interacts directly with the actin-bundling protein plastin-1). For GO Molecular Functions (Fig. 11), three terms were found, only one of which was not also found in the control (unregulated protein group), namely the "glutathione transferase activity" owing to the presence of six different glutathione S-transferase proteins (α3, α4, μ1, π1, θ2, and θ3.) whose abundances were regulated in response to dDAVP (five of six increased). These proteins are believed to be involved in cellular responses to oxidative stress and are regulated in part via transcription factors that bind to so-called "antioxidant regulatory elements" (AREs) (33).

DISCUSSION

Our quantitative proteomics analysis using stable isotope labeling (SILAC) in cultured renal mpkCCD cells (clone 11) confirmed the long-recognized observation that long-term exposure of collecting duct cells to vasopressin results in a large increase in the cellular abundance of aquaporin-2 (6, 34). This response coupled to the ability of vasopressin to stimulate trafficking of aquaporin-2 to the plasma membrane of collecting duct cells accounts for the ability of vasopressin to regulate water excretion. The accompanying transcriptomic analysis (Affymetrix expression arrays) confirmed that vasopressin increases the abundance of aquaporin-2 mRNA (35), and confirms that the increase in aquaporin-2 protein expression owes at least in part to increased mRNA levels, although post-transcriptional mechanisms may also be implicated (36). Therefore, we conclude that the mpkCCD clone 11 cells used in the present study recapitulate the physiological behavior of native collecting duct cells with regard to regulation of aquaporin-2 abundance and supports the use of this model to generalize about other proteins involved in vasopressin action in the collecting duct.

TABLE IV

Abbreviated list of mRNA species increased in abundance in mpkCCD cells in response to long-term (5 days) 0.1 nM dDAVP exposure (limited to those increased by more than 50% or $\log_2$(dDAVP/vehicle) > 0.585). Results are from Affymetrix GeneChip Mouse Genome 430 2.0 Arrays. Shown are $\log_2$ values of dDAVP: vehicle (D/V) ratios. All values reported here were statistically significant versus no change, *i.e.* $\log_2(1)$, by two-tailed t-test ($p < 0.05$).

Gene name	Gene symbol	RefSeq	$\log_2$(D/V) (Mean ± S.E.)
aquaporin 2	*Aqp2*	NM_009699	4.2 ± 0.1
phosphodiesterase 4B, cAMP specific	*Pde4b*	NM_019840	1.8 ± 0.1
complement component 3	*C3*	NM_009778	1.8 ± 0.2
sulfotransferase family 1D, member 1	*Sult1d1*	NM_016771	1.7 ± 0.0
hypothetical protein LOC100044157	*LOC100044157*	XM_001471773	1.7 ± 0.2
gasdermin C2	*Gsdmc2*	NM_177912	1.4 ± 0.1
gasdermin C4	*Gsdmc4*	NM_028992	1.4 ± 0.1
NIPA-like domain containing 1	*Nipal1*	NM_001081205	1.3 ± 0.1
ADP-ribosylation factor-like 4D	*Arl4d*	NM_025404	1.3 ± 0.1
Fc fragment of IgG binding protein	*Fcgbp*	NM_001122603	1.2 ± 0.0
UDP-GlcNAc:betaGal beta-1,3-N-acetylglucosaminyltransferase 7	*B3gnt7*	NM_145222	1.1 ± 0.1
selenoprotein P, plasma, 1, transcript variant 3	*Sepp1*	NM_001042614	1.1 ± 0.1
small proline-rich protein 1A	*Sprr1a*	NM_009264	1.1 ± 0.1
tumor necrosis factor receptor superfamily, 21	*Tnfrsf21*	NM_178589	1.0 ± 0.1
keratin 23	*Krt23*	NM_033373	1.0 ± 0.1
transmembrane protein 178	*Tmem178*	NM_026516	1.0 ± 0.2
gasdermin C	*Gsdmc*	NM_031378	1.0 ± 0.1
lectin, galactose binding, soluble 9, transcript variant 2	*Lgals9*	NM_001159301	1.0 ± 0.2
mucin 4	*Muc4*	NM_080457	0.9 ± 0.1
betacellulin, epidermal growth factor family member	*Btc*	NM_007568	0.9 ± 0.2
alcohol dehydrogenase 1 (class I)	*Adh1*	NM_007409	0.9 ± 0.2
Rho guanine nucleotide exchange factor (GEF) 3	*Arhgef3*	NM_027871	0.8 ± 0.1
G protein-coupled receptor 97	*Gpr97*	NM_173036	0.8 ± 1.0
arginase type II	*Arg2*	NM_009705	0.7 ± 0.1
lipin 2	*Lpin2*	NM_022882	0.7 ± 0.0
degenerative spermatocyte homolog 2 (Drosophila), lipid desaturase	*Degs2*	NM_027299	0.7 ± 0.0
branched chain aminotransferase 1, cytosolic, transcript variant 2	*Bcat1*	NM_007532	0.7 ± 0.1
hypothetical protein LOC52829	*LOC52829*	NM_026821	0.7 ± 0.1
FXYD domain-containing ion transport regulator 4	*Fxyd4*	NM_033648	0.7 ± 0.1
CCAAT/enhancer binding protein (C/EBP), delta	*Cebpd*	NM_007679	0.7 ± 0.1
G protein-coupled receptor, family C, group 5b	*Gprc5b*	NM_022420	0.6 ± 0.1
mitochondrial tumor suppressor 1, nuclear gene encoding mitochondrial protein, transcript variant 3	*Mtus1*	NM_001005864	0.6 ± 0.2
transmembrane protease, serine 4	*Tmprss4*	NM_145403	0.6 ± 0.1
regulator of G-protein signaling 2	*Rgs2*	NM_009061	0.6 ± 0.1
FXYD domain-containing ion transport regulator 2, transcript variant a	*Fxyd2*	NM_007503	0.6 ± 0.1
transmembrane protein 45b	*Tmem45b*	NM_144936	0.6 ± 0.1
lipopolysaccharide binding protein	*Lbp*	NM_008489	0.6 ± 0.0
cyclin Y-like 1	*Ccnyl1*	NM_001097644	0.6 ± 0.1
spermidine/spermine N1-acetyl transferase 1	*Sat1*	NM_009121	0.6 ± 0.1
glutathione S-transferase, α4	*Gsta4*	NM_010357	0.6 ± 0.1
Cbp/p300-interacting transactivator, with Glu/Asp-rich carboxy-terminal domain 4	*Cited4*	NM_019563	0.6 ± 0.1
cytoplasmic FMR1 interacting protein 2	*Cyfip2*	NM_133769	0.6 ± 0.2

When we carried out stable isotope labeling (SILAC) combined with LC-MS/MS for large-scale quantification of proteins in mpkCCD cells, we succeeded in quantifying 786 proteins in at least three separate experiments. Among these, 188 were found to be statistically significantly changed in response to the vasopressin analog dDAVP. Interestingly, among the regulated proteins, only about one-quarter showed corresponding changes in mRNA abundance, even when the analysis was limited to those transcripts abundant enough to be quantified with high statistical power (low false negative rate). This percentage was much lower for down-regulated proteins (6%) than for up-regulated ones (37%). Furthermore, when the analysis was limited to proteins undergoing the largest changes in abundance, at least one-third of responding proteins had no measurable corresponding change in transcript level (Fig. 7*C*). Thus, we conclude that, for the 766 genes that we could quantify with both SILAC LC-MS/MS and Affymetrix microarray, post-transcriptional pro-

TABLE V

Abbreviated list of mRNA species decreased in abundance in mpkCCD cells in response to long-term (5 days) 0.1 nM dDAVP exposure (limited to those decreased by more than 50% $\log_2$(dDAVP/vehicle) < -0.585). Results are from Affymetrix GeneChip Mouse Genome 430 2.0 Arrays. Shown are $\log_2$ values of dDAVP: vehicle (D/V) ratios. All three values reported here were statistically significant versus no change, *i.e.* $\log_2(1)$, by two-tailed *t*-test ($p < 0.05$).

Gene name	Gene symbol	RefSeq	Log_2(D/V) Mean ± S.E.
anthrax toxin receptor 1	Antxr1	NM_054041	−1.3 ± 0.1
RAS-like, family 11, member A	Rasl11a	NM_026864	−0.7 ± 0.1
Fraser syndrome 1 homolog	Fras1	NM_175473	−0.6 ± 0.1

cesses (such as selective regulation of translation and selective regulation of protein degradation) appear to figure importantly in the vasopressin response. The discovery of the mechanisms involved in post-transcriptional regulation of protein abundance depends ultimately on application of methods for large-scale measurement of protein half-life (37) and translation rates (38) in these cells.

Several prior studies have demonstrated imperfect correlation between changes in protein abundance and transcript abundance in response to a variety of stimuli, which is compatible with a role for post-transcriptional regulation of protein abundance for a substantial number of cell types. Most of the early demonstrations were in yeast (1–3). However, more recently, a similar discordance between protein and transcript abundance responses has been noted in mammalian cells, for example, in studies characterizing differentiating embryonic stem cells (39) and the response to therapeutic agents in cancer cells (40). Two aspects of the current study distinguish it from prior studies. First, this study examines the physiological response of mammalian cells to a well known homeostatic signal, specifically exposure of renal collecting ducts to the hormone vasopressin ("antidiuretic hormone"), a response that is reversible and repeatable. Second, the present study, based on state-of-the-art methods for large-scale protein and mRNA quantification, demonstrates an unexpectedly large percentage of proteins that appear to undergo changes in abundance without corresponding changes in mRNA levels. Overall, these findings raise the possibility that normal day-to-day regulation of physiological processes like the one studied here may be accomplished in large part via post-transcriptional mechanisms for altering protein abundance. Further studies are needed to test this idea in other well characterized physiological regulatory systems. Of course, other post-transcriptional processes such as protein phosphorylation and other protein modifications have already been established to be of great importance in the regulation of a variety of physiological processes including the response of the renal collecting duct to vasopressin (41).

Previous studies that have addressed protein-abundance changes in response to long-term exposure to vasopressin in native collecting duct cells using either two-dimensional gels with fluorescent dye labeling (42) or ICAT LC-MS/MS (43) have yielded fewer successful quantifications, owing to technical limitations of the techniques (Fig. 12). Several proteins that were successfully quantified in these previous studies were also quantified in the present study using SILAC LC-MS/MS (Supplemental Table S3). Among these, two changed in all three studies, namely T-plastin (an actin-bundling protein known to be expressed in the renal inner medullary collecting duct) and cathepsin D (a proteolytic enzyme similar to the blood-pressure regulating protein renin). Previous LC-MS/MS profiling studies have demonstrated the presence of cathepsin D in urine (44), suggesting that renal epithelial cells can secrete cathepsin D into the extracellular environment. Indeed, a recent study has demonstrated that cathepsin D in blood plasma can contribute to circulating renin-like activity (45). Additional proteins whose abundances were found to be regulated in the present study and one of two of the prior studies (42, 43) include annexin A2 (*Anxa2*), gelsolin-like capping protein G (*Capg*), carbonic anhydrase 2 (*Car2*), electron-transferring flavoprotein-α (*Etfa*), high density lipoprotein binding protein (*Hdlbp*), keratin 19 (*Krt19*), nucleoside diphosphate kinase B (*Nme2*), protein disulfide isomerase associated 6 (*Pdia6*), peptidylprolyl isomerase B (*Ppib*), transglutaminase 2 C polypeptide (*Tgm2*), and voltage-dependent anion channel 1 (*Vdac1*).

An important product of this study is a new database of the proteome of the mpkCCD clone 11 cells, which has been made freely available to the public at http://dir.nhlbi.nih.gov/papers/lkem/mpkccdproteome/, adding to the existing mpkCCD Transcriptome Database (http://dir.nhlbi.nih.gov/papers/lkem/mpkccdtr/). The new proteome database includes 2990 proteins detected in mpkCCD clone 11 cells and is searchable via the BLAST algorithm to determine whether a given protein is present. This database should be a useful tool for future studies, for example for the choice of targets in knockdown experiments using RNAi techniques.

A fundamental strategy in systems biology is to analyze large-scale proteomic or transcriptomic data to look for common features of the set of regulated proteins or transcripts in order to create hypotheses about the biological processes involved. In this paper, we analyzed the set of proteins whose abundances were significantly altered in mpkCCD cells in response to vasopressin. An analysis of

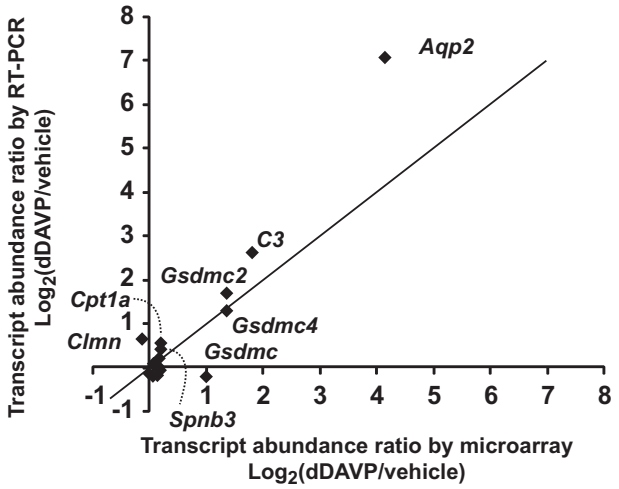

Gene name	Gene symbol	Mean Array	Mean RT-PCR
aquaporin-2	*Aqp2*	4.2*	7.1*
complement C3	*C3*	1.9*	2.7*
gasdermin-C2	*Gsdmc2*	1.4*	1.7*
gasdermin-C4	*Gsdmc4*	1.4*	1.3*
gasdermin-C	*Gsdmc*	1.0*	-0.2
ArfGAP with SH3 domain, ankyrin repeat and PH domain 2	*Asap2*	0.2*	0.3
carnitine O-palmitoyltransferase 1, liver isoform	*Cpt1a*	0.2*	0.6
A-kinase anchor protein 12	*Akap12*	0.2*	0.1
isocitrate dehydrogenase	*Idh1*	0.2*	-0.2
spectrin beta chain, brain 2	*Spnb3*	0.2*	0.5
glutathione S-transferase, theta 3	*Gstt3*	0.2*	-0.1
oxysterol-binding protein-related protein 1	*Osbpl1a*	0.1	-0.2*
MON2 homolog isoform 1	*Mon2*	0.1	0.1
ferritin heavy chain	*Fth1*	0.1	0.1
thyroid hormone receptor interactor 11	*Trip11*	-0.1	-0.2
calmin isoform	*Clmn*	-0.2	0.7

FIG. 6. **Comparison of transcript quantification by Affymetrix microarray with real time RT-PCR.** A 200 ng aliquot total RNA from dDAVP- and vehicle-exposed mpkCCD cells was used for quantification of transcript abundances with real time RT-PCR. *, statistically significant *versus* no change *i.e.* $\log_2$(dDAVP/vehicle) = 0 ($p < 0.05$, $n = 3$). The RefSeq accession numbers are: *Akap12*, NM_031185; *Aqp2*, NM_009699; *Asap2*, NM_001004364; *C3*, NM_009778; *Clmn*, NM_001040682; *Cpt1a*, NM_013495; *Fth1*, NM_010239; *Gsdmc1*, NM_031378; *Gsdmc2*, NM_177912; *Gsdmc4*, XM_001474104; *Gstt3*, NM_133994; *Idh1*, NM_001111320; *Mon2*, NM_153395; *Osbpl1a*, NM_207530; *Spnb3*, NM_021287; and *Trip11*, XM_001001171.

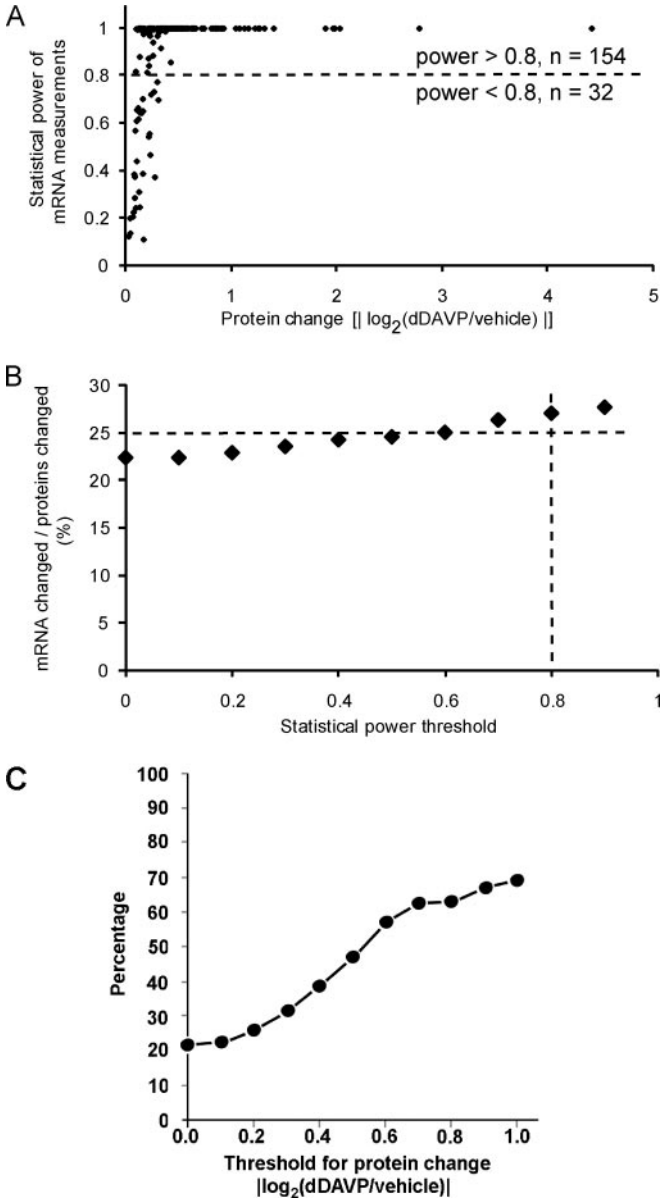

FIG. 7. **Comparison of protein changes with transcript changes.** *A*, Statistical power coefficients (vertical axis) obtained when testing for mRNA abundance differences that are percentage-wise equivalent to the measured protein abundance changes (horizontal axis) for the same gene. Data shown include only proteins whose abundances were significantly altered in response to dDAVP as quantified by SILAC LC-MS/MS. *B*, Percent of the regulated proteins that show corresponding changes in transcript abundances as a function of statistical power threshold. For example, 27% of the regulated proteins have significant changes in the corresponding mRNAs when limited to comparisons with statistical power greater than 0.8. *C*, Percent of regulated proteins that show corresponding changes in transcript abundance as a function of magnitude of protein abundance change threshold.

Gene Ontology "Biological Process" terms enriched in the set of statistically significantly regulated proteins (Fig. 10) identified, at a very high degree of significance, a series of terms pointing to regulation of actin organization. These proteins included gelsolin-like proteins involved in F-actin filament severing and capping as well as a variety of proteins involved in crosslinking F-actin with itself and other proteins (Table VI). Two α-actinin isoforms were up-regulated, α-actinin 1 and 4. These proteins are involved in bundling of F-actin into stress fibers. In addition, three

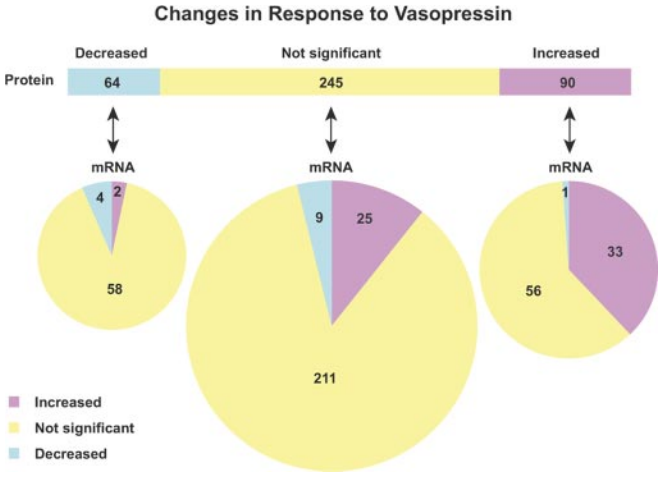

FIG. 8. **Relationship between protein changes and transcript changes in response to vasopressin analog dDAVP.** A total of 399 proteins that have mRNA measurements with statistical powers greater than 0.8 were summarized. Proteins (top bar) are grouped with regard to their responses to dDAVP. Each protein group was then subgrouped with regard to corresponding mRNA changes (bottom pies).

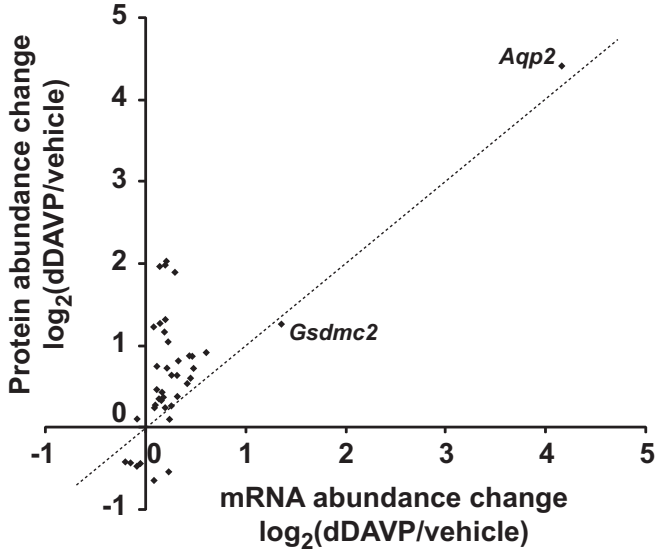

Gene Symbol	Gene Title	mRNA Mean ± SE	Protein Mean ± SE
Aqp2	aquaporin 2	4.15 ± 0.07	4.42 ± 0.51
Gsdmc2	gasdermin C2	1.36 ± 0.15	1.26 ± 0.37
Gsta4	glutathione S-transferase, alpha 4	0.61 ± 0.07	0.91 ± 0.08
Inmt	indolethylamine N-methyltransferase	0.48 ± 0.10	0.72 ± 0.12
Akr1c19	aldo-keto reductase family 1, member C19	0.47 ± 0.08	0.87 ± 0.09
Tgm2	transglutaminase 2, C polypeptide	0.45 ± 0.08	0.60 ± 0.09
Dst	dystonin isoform a	0.44 ± 0.03	0.87 ± 0.22
Abhd14b	abhydrolase domain containing 14b	0.42 ± 0.04	0.53 ± 0.15
Ctsd	cathepsin D precursor	0.33 ± 0.02	0.81 ± 0.15
Cndp2	CNDP dipeptidase 2	0.32 ± 0.07	0.38 ± 0.09
Gmds	GDP-mannose 4,6-dehydratase	0.31 ± 0.01	0.63 ± 0.12
Uap1l1	UDP-N-acteylglucosamine pyrophosphorylase 1	0.29 ± 0.02	1.89 ± 0.18
Lima1	LIM domain and actin binding 1 isoform a	0.26 ± 0.06	0.64 ± 0.02
Ndrg1	N-myc downstream regulated 1	0.26 ± 0.01	0.26 ± 0.05
Krt19	keratin 19	0.24 ± 0.04	0.10 ± 0.02
Gstt2	glutathione S-transferase, theta 2	0.23 ± 0.10	1.04 ± 0.11
Arhgdib	Rho, GDP dissociation inhibitor (GDI) beta	0.23 ± 0.08	-0.54 ± 0.08
H6pd	hexose-6-phosphate dehydrogenase	0.21 ± 0.02	2.03 ± 0.15
Slc25a13	solute carrier family 25, member 13	0.21 ± 0.07	0.72 ± 0.03
Cpt1a	carnitine palmitoyltransferase 1A liver	0.20 ± 0.04	1.98 ± 0.09
Spnb3	spectrin beta 3	0.20 ± 0.05	1.32 ± 0.08
Pgd	phosphogluconate dehydrogenase	0.20 ± 0.02	0.24 ± 0.04
Gstt3	glutathione S-transferase, theta 3	0.19 ± 0.05	1.16 ± 0.21
Actn1	actinin, alpha 1	0.18 ± 0.05	0.37 ± 0.03
Slc25a12	solute carrier family 25, member 12	0.17 ± 0.02	0.43 ± 0.08
Asah1	N-acylsphingosine amidohydrolase 1 precursor	0.16 ± 0.01	0.33 ± 0.02
Akap12	A kinase (PRKA) anchor protein (gravin) 12	0.14 ± 0.04	1.97 ± 0.05
Idh1	isocitrate dehydrogenase 1 (NADP+), soluble	0.14 ± 0.03	1.27 ± 0.08
Krt18	keratin 18	0.13 ± 0.03	0.35 ± 0.06
Lgmn	legumain precursor	0.11 ± 0.06	0.74 ± 0.10
Glud1	glutamate dehydrogenase 1 precursor	0.11 ± 0.03	0.46 ± 0.09
Krt8	keratin complex 2, basic, gene 8	0.10 ± 0.03	0.27 ± 0.07
Sars	seryl-tRNA synthetase	0.09 ± 0.03	0.24 ± 0.06
Gpd1	glycerol-3-phosphate dehydrogenase 1 (soluble)	0.09 ± 0.01	-0.65 ± 0.01
Macf1	microtubule-actin crosslinking factor 1	0.08 ± 0.03	1.23 ± 0.08
Snw1	SKI interacting protein	-0.08 ± 0.02	0.10 ± 0.00
Mcm7	minichromosome maintenance complex component 7	-0.05 ± 0.01	-0.44 ± 0.09
Hsd17b11	estradiol 17-beta-dehydrogenase 11	-0.09 ± 0.03	-0.48 ± 0.06
Anxa6	annexin A6 isoform b	-0.15 ± 0.05	-0.44 ± 0.05
Samd9l	sterile alpha motif domain containing 9like	-0.20 ± 0.04	-0.42 ± 0.07

FIG. 9. **Summary of genes for which changes in protein abundance were accompanied by changes in transcript abundance in response to dDAVP.** Values are mean ± S.E. of log2 values of dDAVP/vehicle abundance ratios.

spectrin isoforms were up-regulated. These proteins are involved in organizing short F-actin filaments into a two-dimensional web abutting the plasma membrane. This actin-spectrin network is instrumental in maintaining plasma membrane shape in part by binding of spectrin to the cytoplasmic tails of integral membrane proteins. The coordinate up-regulation of these α-actinin and spectrin proteins by vasopressin is therefore compatible with a role for vasopressin in regulating F-actin crosslinking with itself and other proteins. A role for regulation of F-actin in the action of vasopressin in collecting duct cells is nominally consistent with prior evidence for vasopressin-induced changes in F-actin distribution in native collecting duct cells (12) and in vasopressin-responsive toad bladder cells (46). Further studies have implicated a known regulator of actomyosin, the small GTPase Rho, in this process (15) and more recently Noda *et al.* have found evidence for local regulation of actin depolymerization near AQP2-containing vesicles through locally activated tropomyosin isoforms (16). Beyond this, the vasopressin-elicited increase in water permeability has been found to be inhibited by the myosin II inhibitor blebbestatin (47), as well as inhibitors of myosin light chain kinase (48), the enzyme responsible for Ca-calmodulin-mediated activation of myosin II. Further studies are needed to address the roles of the specific actin-related proteins found to be regulated by vasopressin in the current study.

Another molecular function found to be enriched in the vasopressin-regulated protein set was "glutathione S-transferase (GST) activity." No less than six GST proteins were increased in abundance in response to long-term exposure to vasopressin. These enzymes conjugate the tri-peptide glutathione to a variety of organic compounds including xenobiotics via glutathione's sulfhydryl group. They have also been found to play a role in cell signaling via binding interactions (49). GST proteins are proposed to be important in the re-

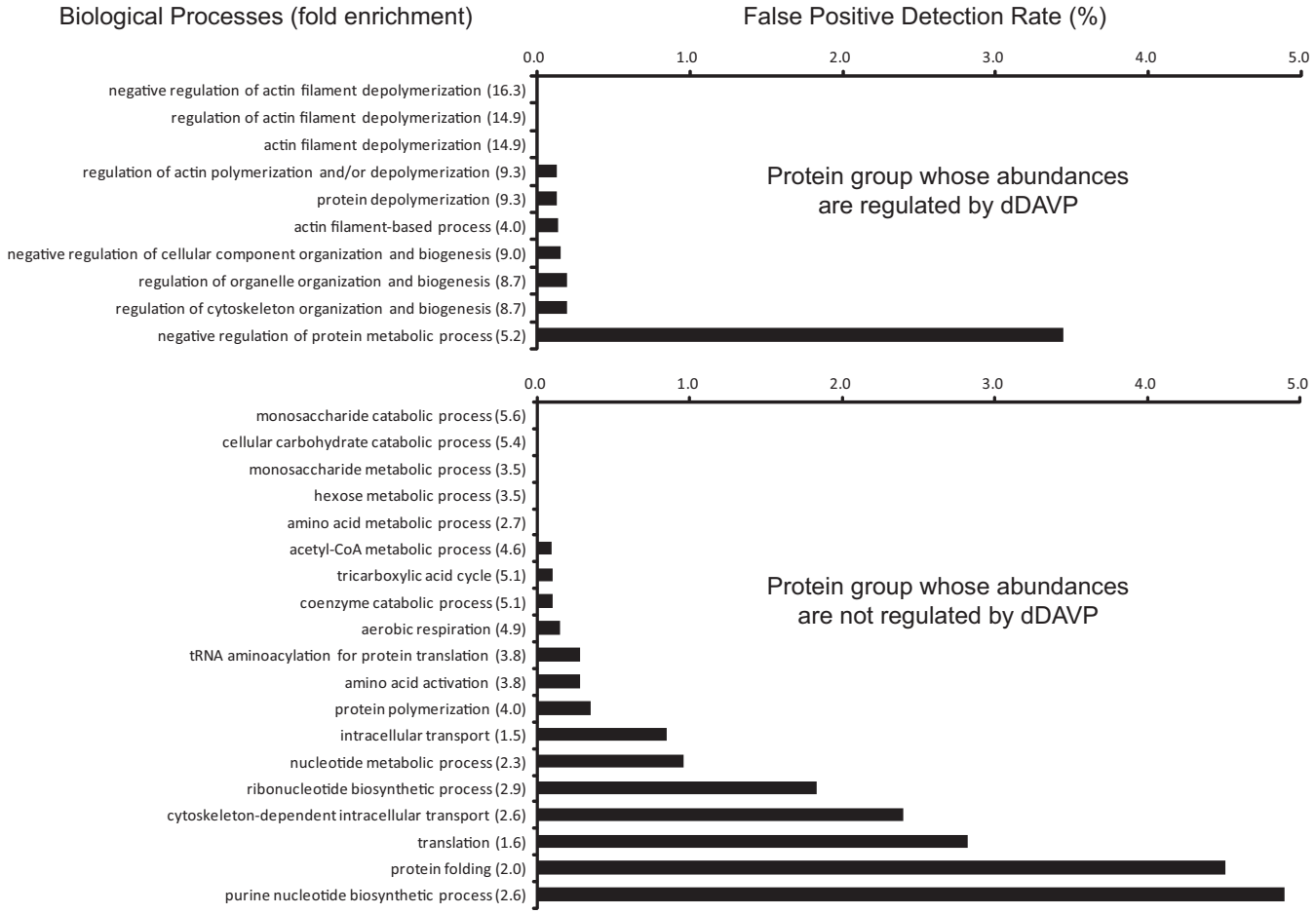

FIG. 10. **Gene Ontology Biological Process analysis for proteins that change in abundances in response to dDAVP.** *Top*, 188 proteins that changed in abundances ($p < 0.05$) in response to dDAVP were used for Gene Ontology Biological Process analysis using the DAVID bioinformatic suite (http://david.abcc.ncifcrf.gov). Enrichment of Biological Process terms in these significantly changed proteins were statistically compared with all transcripts expressed in the mpkCCD cells by Fisher exact test. All GO terms listed were significantly enriched ($p < 0.05$). Fold enrichment is given in parentheses. Bars represent the estimated false positive detection rate. *Bottom*, 598 proteins that did not change in abundances were analyzed the same way, providing a control for the regulated group.

sponse to oxidative stress by removing oxidative by-products and to increase transcriptional regulation resulting of binding of basic helix-loop-helix transcription factors (CREB related factors) to so-called "antioxidant response elements" (33).

As was the case for the distribution of protein abundance changes in response to vasopressin, significant changes in many mRNA species were found, but only a few species showed large changes. Among these, mRNA changes seen for aquaporin-2 exceeded changes seen for all other gene products and these changes were paralleled by corresponding changes in aquaporin-2 protein levels. (Figs. 3 and 9). Thus, the action of vasopressin to regulate the function of collecting duct cells by transcriptional mechanisms appears to be geared largely to regulation of *Aqp2* expression. However, beyond the *Aqp2* gene, there is one additional protein that appears to undergo a substantial increase in abundance as a result of changes in mRNA levels, namely gasdermin C2 (Fig. 9). On the basis of analysis using the Santa Cruz Genome Browser (genome.ucsc.edu), there are four isoforms of gasdermin C in mouse at contiguous positions on chromosome 15, whereas there is only one isoform (gasdermin C1) in other mammalian species including human (NP_113603), rat (P85967), and cow (NP_001039469). Microarray and *in situ* hybridization results show expression of gasdermin C1 in mouse inner medullary collecting ducts, but not in proximal tubules or medullary thick ascending limbs (17, 30), paralleling the pattern of aquaporin-2 expression. Similarly, gasdermin C2/C4 (Affymetrix mouse array probe set ID: 1430641_at) is expressed at fourfold higher level in a mpkCCD cell clone (clone 11) that expresses aquaporin-2 and not in another mpkCCD cell clone (clone 2) that does not express aquaporin-2 (http://dir.nhlbi.nih.gov/papers/lkem/mpkccdtr/). Gasdermin C is one of many genes that lack concrete functional annotations. The increase in gasdermin C2/C4

TABLE VI

Regulated proteins in the significantly enriched "actin cytoskeletal organization and biogenesis" group from Gene Ontology "Biological Process" analysis. Analysis was carried out using online DAVID functional annotation tools (http://david.abcc.ncifcrf.gov/).

Protein name	Gene symbol	RefSeq number	Protein abundance change $\log_2$ (dDAVP/vehicle)[a]	Relative transcript level[b]
gelsolin precursor	Gsn	NP_666232	−0.83 ± 0.04	6.95
integrin beta 1 precursor	Itgb1	NP_034708	−0.31 ± 0.02	4.00
gelsolin-like capping protein isoform 1	Capg	NP_031625	−0.17 ± 0.03	3.52
keratin 19	Krt19	NP_032497	0.10 ± 0.02	7.31
drebrin-like isoform 3	Dbnl	NP_001139780	0.16 ± 0.01	0.99
spectrin beta 2 isoform 2	Spnb2	NP_033286	0.20 ± 0.03	7.66
Wiskott-Aldrich syndrome-like isoform 2	Wasl	NP_001161217	0.23 ± 0.07	4.81
actinin alpha 4	Actn4	NP_068695	0.36 ± 0.05	3.87
actinin, alpha 1	Actn1	NP_598917	0.37 ± 0.03	6.58
flightless I homolog	Flii	NP_071292	0.41 ± 0.05	1.83
radixin isoform b	Rdx	NP_001098087	0.48 ± 0.06	3.30
spectrin alpha 2	Spna2	NP_001070022	0.58 ± 0.04	7.06
spectrin beta 3	Spnb3	NP_067262	1.32 ± 0.08	1.84

[a] Values are mean ± S.E. ($p < 0.05$ versus $\log_2$(dDAVP/vehicle) = 0).

[b] Values are median normalized transcript levels from mpkCCD Transcriptome Database (http://dir.nhlbi.nih.gov/papers/lkem/mpkccdtr/).

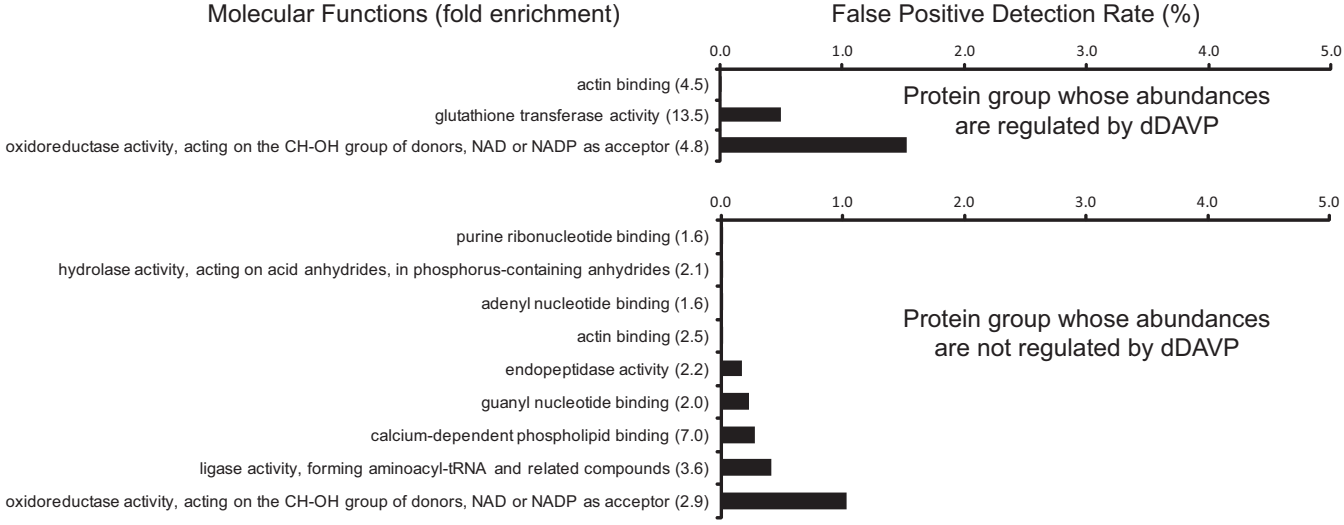

FIG. 11. **Gene Ontology Molecular Function analysis for proteins that change in abundances in response to dDAVP.** Top, 188 proteins that changed in abundance ($p < 0.05$) in response to dDAVP were used for Gene Ontology Molecular Function analysis using the DAVID bioinformatic suite (http://david.abcc.ncifcrf.gov). Enrichment of Molecular Function terms in these significantly changed proteins were statistically compared with all transcripts expressed in the mpkCCD cells by Fisher exact test (All GO terms listed were significantly enriched at $p < 0.05$.). Fold enrichment is given in parentheses. Bars represent the estimated false positive detection rate. Bottom, 598 proteins that did not change in abundance were analyzed the same way, providing a control for the regulated group.

mRNA was confirmed by real time RT-PCR in separate experiments (Fig. 6). Changes in mRNA levels can occur via changes in transcription rate or changes in transcript degradation rate, and we have no information presently telling us which occurs.

Conserved transcription factor binding site analysis (*Genomatix* software) of 1000 bp of the 5′-flanking region of the gasdermin C2 gene *versus* the *Aqp2* gene in four species (human, dog, rat, and mouse) reveals 20 putative transcription factor binding motifs in common (Supplemental Fig. S5, Supplemental Table S6). Among these motifs, four of them (V$NFKB, V$IRFF, V$EBOX, and V$AP2F) are known or predicted to bind transcription factors (*Nfkb2*, *Irf3*, *Myc*, and *Tcfap2a*) that are expressed in mpkCCD cells and the native inner medullary collecting duct cells according to our previous transcriptomic analyses (17, 30). These transcription factors could potentially be involved in regulation of *Aqp2* and *Gsdmc2* gene expression. In fact, the transcription factor NFkB (gene symbol: *Nfkb2*) has been previously shown to decrease *Aqp2* gene expression in the original mpkCCD cells (50). Its role in gasdermin C2 mRNA and protein regulation requires further experiments. Analysis of the 3′-untranslated regions of aquaporin-2 and gasdermin C2 transcripts does not reveal any shared conserved putative miRNA binding site, based on TargetScanMouse (http://www.targetscan.org) and microRNA.org (http://www.microrna.org) online tools. Thus, we

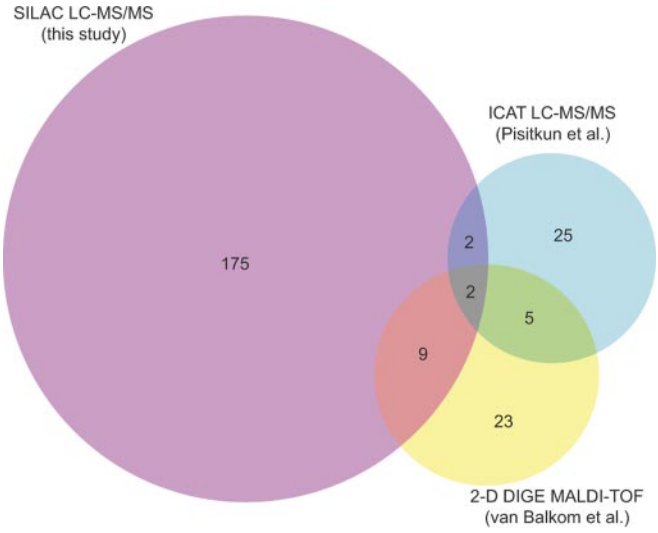

FIG. 12. **Comparison of regulated-proteins with those found in two prior proteomic studies of long-term vasopressin effects.** Prior studies that have addressed protein abundance changes in response to long-term exposure to vasopressin in native collecting duct cells used either two-dimensional gels with fluorescent dye labeling (42) or ICAT LC-MS/MS (43) for quantification. Integers represent the number of proteins found to be significantly changed in abundance in each subsection of the Venn diagram (total for this study, 188 proteins).

cannot make any judgment presently about the mechanism by which gasdermin C2 mRNA levels change in response to vasopressin.

Acknowledgments—These funding organizations had no role in study design, data collection and analysis, decision to publish, or preparation of the manuscript. Mass spectrometry was done in the NHLBI Proteomics Core Facility (Marjan Gucek, Director). The microarray analysis utilized the NHLBI Gene Expression Core Facility (Nalini Raghavachari, Director). We thank R. Lance Miller for suggestions regarding the study, Wells Wu for help with MRM analysis, and Panapat Uawithya for his assistance on microarray experiments and data analysis.

* The work was funded by the Division of Intramural Research, NHLBI (project ZO1-HL001285, MAK). SK was supported by the International Society of Nephrology, the Kidney Foundation of Thailand, and the Faculty of Medicine, Thammasat University, Thailand.

S This article contains supplemental Figs. 1–5 and Tables 1–6.

§ To whom correspondence should be addressed: Institute of Biochemistry and Molecular Biology, National Taiwan University College of Medicine, Rm 816, No. 1 Ren-Ai Road Section 1, Taipei 100, Taiwan. Tel.: +8862 2312-3456 ext 88216; Fax: +8862 2391–5295; E-mail: mjyu@ntu.edu.tw.

REFERENCES

1. Gygi, S. P., Rochon, Y., Franza, B. R., and Aebersold, R. (1999) Correlation between protein and mRNA abundance in yeast. *Mol. Cell. Biol.* **19,** 1720–1730
2. Ideker, T., Thorsson, V., Ranish, J. A., Christmas, R., Buhler, J., Eng, J. K., Bumgarner, R., Goodlett, D. R., Aebersold, R., and Hood, L. (2001) Integrated genomic and proteomic analyses of a systematically perturbed metabolic network. *Science* **292,** 929–934
3. Washburn, M. P., Koller, A., Oshiro, G., Ulaszek, R. R., Plouffe, D., Deciu, C., Winzeler, E., and Yates, J. R., 3rd. (2003) Protein pathway and complex clustering of correlated mRNA and protein expression analyses in *Saccharomyces cerevisiae*. *Proc. Natl. Acad. Sci. U.S.A.* **100,** 3107–3112
4. Nielsen, S., Frøkiaer, J., Marples, D., Kwon, T. H., Agre, P., and Knepper, M. A. (2002) Aquaporins in the kidney: from molecules to medicine. *Physiol. Rev.* **82,** 205–244
5. Wall, S. M., Han, J. S., Chou, C. L., and Knepper, M. A. (1992) Kinetics of urea and water permeability activation by vasopressin in rat terminal IMCD. *Am. J. Physiol.*. **262,** F989-F998
6. DiGiovanni, S. R., Nielsen, S., Christensen, E. I., and Knepper, M. A. (1994) Regulation of collecting duct water channel expression by vasopressin in Brattleboro rat. *Proc.Natl Acad. Sci. U.S.A.* **91,** 8984–8988
7. Hoffert, J. D., Chou, C. L., Fenton, R. A., and Knepper, M. A. (2005) Calmodulin is required for vasopressin-stimulated increase in cyclic AMP production in inner medullary collecting duct. *J. Biol. Chem.* **280,** 13624–13630
8. Yip, K. P. (2002) Coupling of vasopressin-induced intracellular Ca2+ mobilization and apical exocytosis in perfused rat kidney collecting duct. *J. Physiol*. **538,** 891–899
9. Pisitkun, T., Jacob, V., Schleicher, S. M., Chou, C. L., Yu, M. J., and Knepper, M. A. (2008) Akt and ERK1/2 pathways are components of the vasopressin signaling network in rat native IMCD. *Am. J. Physiol. Renal Physiol.* **295,** F1030-F1043
10. Chou, C. L., Yip, K. P., Michea, L., Kador, K., Ferraris, J. D., Wade, J. B., and Knepper, M. A. (2000) Regulation of aquaporin-2 trafficking by vasopressin in renal collecting duct: Roles of ryanodine-sensitive Ca^{2+} stores and calmodulin. *J. Biol. Chem.* **275,** 36839–36846
11. Chou, C. L., Christensen, B. M., Frische, S., Vorum, H., Desai, R. A., Hoffert, J. D., de, Lanerolle, P., Nielsen, S., and Knepper, M. A. (2004) Non-muscle myosin II and myosin light chain kinase are downstream targets for vasopressin signaling in the renal collecting duct. *J. Biol. Chem.* **279,** 49026–49035
12. Simon, H., Gao, Y., Franki, N., and Hays, R. M. (1993) Vasopressin depolymerizes apical F-actin in rat inner medullary collecting duct. *Am. J.Physiol.*. **265,** C757-C762
13. Grantham, J. J. (1970) Vasopressin: Effect on deformability of urinary surface of collecting duct cells. *Science* **168,** 1093–1095
14. Klussmann, E., Tamma, G., Lorenz, D., Wiesner, B., Maric, K., Hofmann, F., Aktories, K., Valenti, G., and Rosenthal, W. (2001) An inhibitory role of Rho in the vasopressin-mediated translocation of aquaporin-2 into cell membranes of renal principal cells. *J. Biol. Chem.* **276,** 20451–20457
15. Tamma, G., Klussmann, E., Procino, G., Svelto, M., Rosenthal, W., and Valenti, G. (2003) cAMP-induced AQP2 translocation is associated with RhoA inhibition through RhoA phosphorylation and interaction with RhoGDI. *J. Cell. Sci.* **116,** 1519–1525
16. Noda, Y., Horikawa, S., Kanda, E., Yamashita, M., Meng, H., Eto, K., Li, Y., Kuwahara, M., Hirai, K., Pack, C., Kinjo, M., Okabe, S., and Sasaki, S. (2008) Reciprocal interaction with G-actin and tropomyosin is essential for aquaporin-2 trafficking. *J. Cell. Biol.* **182,** 587–601
17. Yu, M. J., Miller, R. L., Uawithya, P., Rinschen, M. M., Khositseth, S., Braucht, D. W., Chou, C. L., Pisitkun, T., Nelson, R. D., and Knepper, M. A. (2009) Systems-level analysis of cell-specific AQP2 gene expression in renal collecting duct. *Proc. Natl. Acad. Sci. U.S.A.* **106,** 2441–2446
18. Ong, S. E., Blagoev, B., Kratchmarova, I., Kristensen, D. B., Steen, H., Pandey, A., and Mann, M. (2002) Stable isotope labeling by amino acids in cell culture, SILAC, as a simple and accurate approach to expression proteomics. *Mol. Cell. Proteomics.* **1,** 376–386
19. Pisitkun, T., Jacob, V., Schleicher, S. M., Chou, C. L., Yu, M. J., and Knepper, M. A. (2008) Akt and ERK1/2 pathways are components of the vasopressin signaling network in rat native IMCD. *Am. J. Physiol. Renal Physiol*. **295,** F1030-F1043
20. Hoffert, J. D., Fenton, R. A., Moeller, H. B., Simons, B., Tchapyjnikov, D., McDill, B. W., Yu, M. J., Pisitkun, T., Chen, F., and Knepper, M. A. (2008) Vasopressin-stimulated increase in phosphorylation at Ser269 potentiates plasma membrane retention of aquaporin-2. *J. Biol. Chem.* **283,** 24617–24627
21. Yu, M. J., Pisitkun, T., Wang, G., Aranda, J. F., Gonzales, P. A., Tchapyjnikov, D., Shen, R. F., Alonso, M. A., and Knepper, M. A. (2008) Large-scale quantitative LC-MS/MS analysis of detergent-resistant membrane proteins from rat renal collecting duct. *Am. J. Physiol. Cell Physiol.* 101,

13368–13373
22. van Hoof, D., Pinkse, M. W., Oostwaard, D. W., Mummery, C. L., Heck, A. J., and Krijgsveld, J. (2007) An experimental correction for arginine-to-proline conversion artifacts in SILAC-based quantitative proteomics. *Nat. Methods*. **4,** 677–678
23. Pisitkun, T., Shen, R. F., and Knepper, M. A. (2004) Identification and proteomic profiling of exosomes in human urine. *Proc. Natl. Acad. Sci. U.S.A.* **101,** 13368–13373
24. Eng, J. K., McCormack, A. L., and Yates, J. R., III. (1994) An approach to correlate tandem mass spectral data of peptides with amino acid sequences in a protein database. *J. Am. Soc. Mass. Spectrom.* **5,** 976–989
25. Tanner, S., Shu, H., Frank, A., Wang, L. C., Zandi, E., Mumby, M., Pevzner, P. A., and Bafna, V. (2005) InsPecT: identification of posttranslationally modified peptides from tandem mass spectra. *Anal. Chem.* **77,** 4626–4639
26. Geer, L. Y., Markey, S. P., Kowalak, J. A., Wagner, L., Xu, M., Maynard, D. M., Yang, X., Shi, W., and Bryant, S. H. (2004) Open mass spectrometry search algorithm. *J. Proteome. Res.* **3,** 958–964
27. Elias, J. E., and Gygi, S. P. (2007) Target-decoy search strategy for increased confidence in large-scale protein identifications by mass spectrometry. *Nat. Methods*. **4,** 207–214
28. Tchapyjnikov, D., Li, Y., Pisitkun, T., Hoffert, J. D., Yu, M. J., and Knepper, M. A. (2010) Proteomic profiling of nuclei from native renal inner medullary collecting duct cells using LC-MS/MS. *Physiol. Genomics* **40,** 167–183
29. Wang, G., Wu, W. W., Pisitkun, T., Hoffert, J. D., Knepper, M. A., and Shen, R. F. (2006) Automated quantification tool for high-throughput proteomics using stable isotope labeling and LC-MSn. *Anal. Chem.* **78,** 5752–5761
30. Uawithya, P., Pisitkun, T., Ruttenberg, B. E., and Knepper, M. A. (2008) Transcriptional profiling of native inner medullary collecting duct cells from rat kidney. *Physiol. Genomics* **32,** 229–253
31. Wang, G., Wu, W. W., Pisitkun, T., Hoffert, J. D., Knepper, M. A., and Shen, R. F. (2006) Automated quantification tool for high-throughput proteomics using stable isotope labeling and LC-MSn. *Anal. Chem.* **78,** 5752–5761
32. Huang, da, W., Sherman, B. T., and Lempicki, R. A. (2009) Systematic and integrative analysis of large gene lists using DAVID bioinformatics resources. *Nat. Protoc.* **4,** 44–57
33. Nguyen, T., Sherratt, P. J., and Pickett, C. B. (2003) Regulatory mechanisms controlling gene expression mediated by the antioxidant response element. *Annu. Rev. Pharmacol. Toxicol.* **43,** 233–260
34. Hasler, U., Mordasini, D., Bens, M., Bianchi, M., Cluzeaud, F., Rousselot, M., Vandewalle, A., Feraille, E., and Martin, P. Y. (2002) Long term regulation of aquaporin-2 expression in vasopressin-responsive renal collecting duct principal cells. *J. Biol. Chem.* **277,** 10379–10386
35. Ecelbarger, C. A., Nielsen, S., Olson, B. R., Murase, T., Baker, E. A., Knepper, M. A., and Verbalis, J. G. (1997) Role of renal aquaporins in escape from vasopressin-induced antidiuresis in rat. *J.Clin. Invest.* **99,** 1852–1863
36. Brooks, H. L., Ageloff, S., Kwon, T. H., Brandt, W., Terris, J. M., Seth, A., Michea, L., Nielsen, S., Fenton, R., and Knepper, M. A. (2003) cDNA array identification of genes regulated in rat renal medulla in response to vasopressin infusion. *Am. J. Physiol. Renal Physiol*. **284,** F218-F228
37. Yen, H. C., Xu, Q., Chou, D. M., Zhao, Z., and Elledge, S. J. (2008) Global protein stability profiling in mammalian cells. *Science* **322,** 918–923
38. Hendrickson, D. G., Hogan, D. J., McCullough, H. L., Myers, J. W., Herschlag, D., Ferrell, J. E., and Brown, P. O. (2009) Concordant regulation of translation and mRNA abundance for hundreds of targets of a human microRNA. *PLoS. Biol.* **7,** e1000238
39. Unwin, R. D., Smith, D. L., Blinco, D., Wilson, C. L., Miller, C. J., Evans, C. A., Jaworska, E., Baldwin, S. A., Barnes, K., Pierce, A., Spooncer, E., and Whetton, A. D. (2006) Quantitative proteomics reveals posttranslational control as a regulatory factor in primary hematopoietic stem cells. *Blood* **107,** 4687–4694
40. Harris, M. N., Ozpolat, B., Abdi, F., Gu, S., Legler, A., Mawuenyega, K. G., Tirado-Gomez, M., Lopez-Berestein, G., and Chen, X. (2004) Comparative proteomic analysis of all-trans-retinoic acid treatment reveals systematic posttranscriptional control mechanisms in acute promyelocytic leukemia. *Blood* **104,** 1314–1323
41. Rinschen, M. M., Yu, M. J., Wang, G., Boja, E. S., Hoffert, J. D., Pisitkun, T., and Knepper, M. A. (2010) Quantitative phosphoproteomic analysis reveals vasopressin V2-receptor-dependent signaling pathways in renal collecting duct cells. *Proc. Natl. Acad. Sci. U.S.A.* **107,** 3882–3887
42. van Balkom, B. W., Hoffert, J. D., Chou, C. L., and Knepper, M. A. (2004) Proteomic analysis of long-term vasopressin action in the inner medullary collecting duct of the Brattleboro rat. *Am. J. Physiol. Renal Physiol*. **286,** F216-F224
43. Pisitkun, T., Bieniek, J., Tchapyjnikov, D., Wang, G., Wu, W. W., Shen, R. F., and Knepper, M. A. (2006) High-Throughput Identification of IMCD Proteins Using LC-MS/MS. *Physiol Genomics* **25,** 263–276
44. Gonzales, P. A., Pisitkun, T., Hoffert, J. D., Tchapyjnikov, D., Star, R. A., Kleta, R., Wang, N. S., and Knepper, M. A. (2009) Large-scale proteomics and phosphoproteomics of urinary exosomes. *J. Am. Soc. Nephrol.* **20,** 363–379
45. Naseem, R. H., Hedegard, W., Henry, T. D., Lessard, J., Sutter, K., and Katz, S. A. (2005) Plasma cathepsin D isoforms and their active metabolites increase after myocardial infarction and contribute to plasma renin activity. *Basic Res. Cardiol.* **100,** 139–146
46. Ding, G. H., Franki, N., Condeelis, J., and Hays, R. M. (1991) Vasopressin depolymerizes F-actin in toad bladder epithelial cells. *Am. J. Physiol.* **260,** C9–16
47. Chou, C. L., Yu, M. J., Kassai, E. M., Morris, R. G., Hoffert, J. D., Wall, S. M., and Knepper, M. A. (2008) Roles of basolateral solute uptake via NKCC1 and of myosin II in vasopressin-induced cell swelling in inner medullary collecting duct. *Am. J. Physiol. Renal Physiol*. **295,** F192-F201
48. Chou, C. L., Christensen, B. M., Frische, S., Vorum, H., Desai, R. A., Hoffert, J. D., de Lanerolle, P., Nielsen, S., and Knepper, M. A. (2004) Non-muscle myosin II and myosin light chain kinase are downstream targets for vasopressin signaling in the renal collecting duct. *J. Biol. Chem.* **279,** 49026–49035
49. Wu, Y., Fan, Y., Xue, B., Luo, L., Shen, J., Zhang, S., Jiang, Y., and Yin, Z. (2006) Human glutathione S-transferase P1–1 interacts with TRAF2 and regulates TRAF2-ASK1 signals. *Oncogene* **25,** 5787–5800
50. Hasler, U., Leroy, V., Jeon, U. S., Bouley, R., Dimitrov, M., Kim, J. A., Brown, D., Kwon, H. M., Martin, P. Y., and Féraille, E. (2008) NF-kappaB Modulates aquaporin-2 transcription in renal collecting duct principal cells. *J. Biol. Chem.* **283,** 28095–28105